Chapter 4

A new three-dimensionally modulated Twist Grain Boundary phase

4.1 Introduction

Twist Grain Boundary (TGB) phases are liquid crystalline analogues of the Abrikosov phase exhibited by type-I1 superconductors. Some of these remarkable structures were theoretically predicted based on an analogy between the two seemingly very different systems. The similarities between the nematic to smectic-A transition and the normal metal to superconductor transition were first pointed out by de Gennes [10]. He recognised the striking resemblance between the Landau-Ginzburg free energy expressions describing these two systems. Some relevant aspects of this analogy are discussed below.

As described in the first chapter, the smectic layering can be described by a mass-density wave along the layer normal direction ($\hat{\mathbf{z}}$). If ρ_o is the average mass-density,

$$\rho(z) = \rho_o + \psi e^{i\mathbf{q_A}\cdot\mathbf{z}} , \tag{4.1}$$

where $q_A = 2\pi/d$; d is the layer spacing. The smectic-A order parameter can be expressed as

$$\psi = |\psi_o| e^{-i\phi} . \tag{4.2}$$

The order parameter is zero in the nematic phase and becomes non-zero below the

nematic to smectic-A (NA) transition point.

The Landau-Ginzburg free energy expression describing the NA transition can then be written as [10, 6]

$$F_{NA} = \int d^3x \left[r|\psi|^2 + \frac{g}{2}|\psi|^4 + C_{\|} \left| \frac{\partial \psi}{\partial z} \right|^2 + C_{\perp} |(\nabla_{\perp} - iq_A \delta n_{\perp})| \psi|^2 \right] + F_{el} \,, \quad (4.3)$$

where F_{el} is the energy cost for the distortions in the Frank-director field. The $C_{\perp}$ term is written in a covariant form because rigid rotations of the smectic layers and the director do not cost any elastic energy. In writing Eq. ***4.3*** it has been assumed that the deviations in $\hat{\mathbf{n}}$ from the $\hat{\mathbf{z}}$ direction are small. The F_{el} part of Eq. ***4.3*** is

$$F_N = \frac{1}{2} \int d^3x \left[K_{11} (\boldsymbol{\nabla} \cdot \hat{\mathbf{n}})^2 + K_{22} (\hat{\mathbf{n}} \cdot \boldsymbol{\nabla} \times \hat{\mathbf{n}})^2 + K_{33} (\hat{\mathbf{n}} \times \boldsymbol{\nabla} \times \hat{\mathbf{n}})^2 \right] \,. \quad (4.4)$$

In Eq. ***4.3,*** the first term which is quadratic in ψ drives the NA transition. Its coefficient is expressed as $r = \boldsymbol{a}(\boldsymbol{T} - T_{NA})$, where T_{NA} is the transition temperature and $\boldsymbol{a}$ is a constant. The term quartic in ψ is required for stability. The terms with coefficients $C_{\|}$ and $C_{\perp}$ give the energy cost for creating gradients in the order parameter. Assuming $C_{\|} = C_{\perp} = \boldsymbol{C}$ and $K_{11} = K_{22} = K_{33} = \mathrm{K}$, Eq. ***4.3*** reduces to

$$F_{NA} = \int d^3x \left[r|\psi|^2 + \frac{g}{2}|\psi|^4 + C|(\boldsymbol{\nabla} - iq_A \hat{\mathbf{n}})\psi|^2 + \boldsymbol{K}\,(\boldsymbol{V} \,.\, \hat{\mathbf{n}})^2 + \boldsymbol{K}\,(\boldsymbol{V} \times \hat{\mathbf{n}})^2 \right] \,. \quad (4.5)$$

The form of Eq. ***4.5*** is almost the same as that for the Landau-Ginzburg free energy expression describing the normal metal to the superconductor transition [10, 1, 42], which is written as

$$F_{NS} = \int d^3x \left[r|\psi|^2 + \frac{g}{2}|\psi|^4 + \frac{1}{m} \left| \left(\hbar \boldsymbol{\nabla} - i \frac{q}{c} \mathbf{A} \right) \psi \right|^2 + \frac{1}{8\pi\mu} (\boldsymbol{\nabla} \times \mathbf{A})^2 \right] \,. \quad (4.6)$$

In the above equation, ψ is the superconductor 'gap' order parameter, **A** the magnetic vector potential, m the particle mass, q the charge of the particle, c the speed of light, $\hbar$ the Plank's constant and μ the magnetic permittivity.

A comparison of Eq. ***4.5*** and Eq. ***4.6*** reveals the following analogies: Both systems are described by complex order parameters, the Cooper-pair wave function

in the case of superconductors and the mass-density wave normal to the layers in the case of smectic-A. The nematic director, ii, is analogous to the vector potential A and twist/bend (V x ii) deformations to the magnetic induction (B = V x A). There is, however, no anolog of the splay deformation in the case of superconductors since V . A = 0.

Just as superconductors expel magnetic lines of force, smectic liquid crystals expel twist and bend deformations of the Frank-director. This is because these deformations are necessarily associated with layer spacing variations which are energetically very expensive.

Superconductors are classified into two types depending on their behaviour under an external magnetic field. The behaviour exhibited depends on the ratio of their penetration depth, A, to their coherence length, ξ (see Fig. 4.1). This ratio, $\kappa = \lambda/\xi$ is known as the Ginzburg parameter. If $\kappa < 1/\sqrt{2}$, the superconductor expels the field completely (Meissner effect) up to a critical value of the field above which it transforms to a normal metal. Such materials are called type-I superconductors. If, on the other hand, $\kappa > 1/\sqrt{2}$, there can be an intermediate state between the perfect superconductor and the normal metal in which magnetic flux lines penetrate the superconductor in the form of a triangular lattice of quantised flux tubes. This phase is known as the Abrikosov phase and materials exhibiting this state are known as type-I1 superconductors.

Based on the similarities described above, de Gennes argued that like superconductors smectic-A liquid crystals can also be classified into type-I and type-I1 smectics based on their response to a bending or twisting stress. In smectic-A, however, there are two order parameter coherence lengths, $\xi_{||,\perp} = (C_{||,\perp}/|r|)^{1/2}$ and four penetration lengths $\lambda^{2,3}_{||,\perp} = (K_{22,33}u/C_{||,\perp}|r|)^{1/2}$, where **2,3** stands for twist,bend and $||, \perp$ for directions which are parallel and perpendicular to the layer normal, respectively. Thus liquid crystals, due to their highly anisotropic character, are much

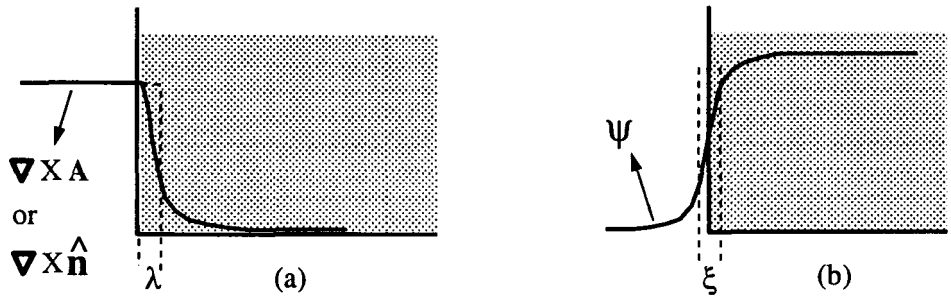

Figure 4.1: Pictorial representation of the definitions of the two lengths λ and ξ. The dotted region represents smectic-A/superconductor and the blank region nematic/normal metal.

---

more complex than superconductors. Assuming $\xi_{\|,\perp} \equiv \xi$ and $\lambda_{\|,\perp}^{2,3} \equiv \lambda$, the ratio of the two $\kappa = \lambda/\xi$ is the analogue of the Ginzburg parameter. If $\kappa < 1/\sqrt{2}$, the smectic-A resists twist/bend deformations until a critical value of the stress at which it melts into a nematic. Then it is called a type-I smectic. If the smectic is type-11, $\kappa > 1/\sqrt{2}$, the twist/bend deformations can penetrate the smectic in the form of screw/edge dislocations when the stress is increased beyond a critical value. Thus, screw/edge dislocations are the liquid crystalline analogues of the magnetic flux tubes in superconductors.

In the case of liquid crystals there is another interesting possibility. ie., instead of applying an externally imposed twist deformation, the medium can be made chiral. This can be done either by making the molecules chiral or by doping the smectic with a chiral material. In such a system there is an intrinsic tendency for creating twist deformations due to chiral interactions. The nematic is now replaced by a cholesteric phase. The Frank free energy expression for the cholesteric is

$$F_{N^*} = F_{el} + \int d^3x \, \Lambda(\hat{\mathbf{n}} \cdot \nabla \times \hat{\mathbf{n}}), \tag{4.7}$$

where A is referred to as the 'chiral strength' of the medium. At lower temperatures, when the smectic order sets in, there are two possibilities. If the smectic is type-I the lower temperature phase is the usual smectic-A phase. But if the smectic

is type-11, then there can be a 'twisted smectic phase' between the cholesteric and the smectic-A phases. This intermediate phase is formed by a proliferation of screw dislocations. Screw dislocations cause the smectic layering to tilt with respect to the dislocation line. This in turn results in a twist deformation in the Frank-director across the dislocation line. The screw dislocation ridden state can be expected to be stable if the chiral energy gained by twisting the Frank-director exceeds the elastic energy cost for creating the dislocations.

The simplest structure to imagine is perhaps a smectic with a lattice of parallel screw dislocations as in the case of superconductors. But, Sethna has pointed out that such a configuration with parallel screw dislocations will cost an energy which diverges with system size. His argument which is discussed in Ref. [8] is as follows: Consider a spatially uniform lattice of parallel screw dislocations with an area density n_A. A circular contour of radius R will enclose $\pi R^2 n_A$ dislocations. If $\boldsymbol{u}$ is the displacement of the smectic layers, $\int \mathrm{dl} \cdot \boldsymbol{\nabla u} = (\pi R^2 n_A) d$, where d is the smectic layer spacing. This gives an average $|\boldsymbol{\nabla} u|$ which is equal to $\frac{1}{2} R d n_A$. This implies that $|\boldsymbol{\nabla} u| \to \infty$ as R $\to \infty$ and hence does not have a well defined thermodynamic limit.

4.1.1 The Twist Grain Boundary phases

The detailed structure of a thermodynamically stable phase analogous to the Abrikosov phase was worked out by Renn and Lubensky [8]. Some of the details of their calculations will be presented in the next chapter. They realised that the difficulty mentioned above can be overcome if the screw dislocations are confined to a parallel set of planes as shown in Fig. **4.2.** Each plane contains a linear array of parallel screw dislocations and is referred to as a Twist Grain Boundary. Such an array of screw dislocations will cause the smectic layers on either sides of the grain boundary to be oriented at an angle with respect to each other [7]. Thus, this new phase, which they called the Twist Grain Boundary (TGB) phase, consists of a twisted

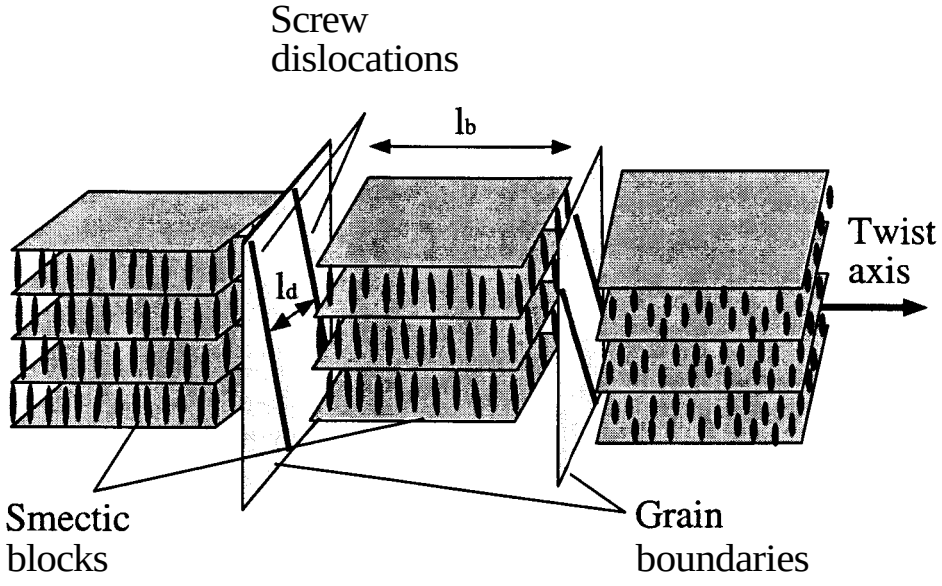

Figure 4.2: Schematic diagram of the TGB_A structure which was predicted by Renn and Lubensky and discovered by Goodby et *al.* The block size l_b and the spacing between screw dislocations within a grain boundary l_d are of the order of a few hundred angstroms.

---

arrangement of more or less uniform smectic regions separated by highly distorted grain boundaries. There is a twist deformation in the Rank-director across each grain boundary. The TGB structure becomes stable compared to that of smectic-A when chiral energy gained from this twist exceeds the energy cost of introducing the screw dislocations. Since the smectic blocks are SmA-like, this TGB phase is usually called the TGB_A phase to distiguish it from the other TGB phases.

The first experimental confirmation of the TGB_A structure was made by Goodby et *al.* [9]. The structure was determined by microscopic studies on the texture and xray diffraction studies. Later, freeze-fracture studies unambiguously established the existence of arrays of screw dislocations in this structure [43].

Unlike superconductors, smectic liquid crystals can exhibit other modifications depending on the structure within the smectic blocks. According to the theoretical prediction, the structure of the TGB_C phase differs from that of the TGB_A phase in that the molecules are now tilted with respect to the layer normal. The tilt

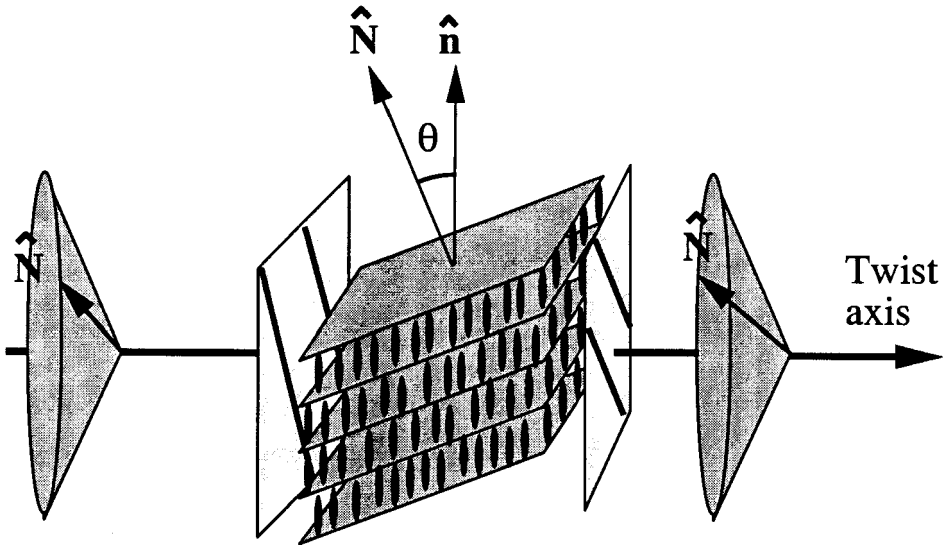

Figure 4.3: Schematic diagram of the TGB_C structure seen by the Bourdeaux group. Unlike the TGB_A, in this case the smectic layers are tilted with respect to the grain boundaries. On passing from one block to another, the layer normal, N, precesses about a cone.

---

direction is supposed to be parallel to the grain boundaries so that the twist is about an axis orthogonal to the Frank-director. But in the experimentally observed structure it was seen that the *smectic layers* are tilted with respect to the grain boundary by an angle which is approximately equal to the smectic-C tilt angle [44] (Fig. 4.3). Adjacent blocks are rotated about an axis normal to the grain boundary such that the smectic layer normal, N, precesses about a cone on going from block to block. Note that the twist is again perpendicular to the Frank-director like in the cholesterics and the TGB_A phases, as this maximises the twist distortion across the grain boundaries.

Apart from these structures, Renn has also predicted a TGB_{C^*} phase [45]. In this the smectic blocks are smectic-C^*-like. The schematic diagram of this structure reproduced from Ref.[45] is shown in Fig. 4.4. Kuczynski and Stegemeyer [46, 47] have reported the observation of a new TGB phase in a binary mixture, which they speculated to be the TGB_{C^*} phase predicted by Renn. Their speculation was based on the unusual spiral filamentary texture exhibited by this phase. No detailed

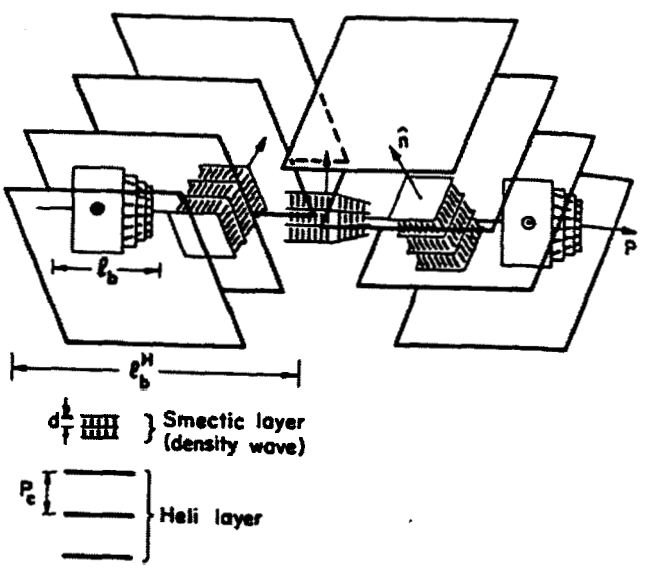

Figure 4.4: The TGB_{C^*} structure proposed by Renn (reproduced from, Ref. [45] It consists of a twisted stack of helislabs superimposed on a twisted stack of smectic slabs. The helilayers which constitutes the helislabs are planes of constant orientation of the c-vector.

experiments were done in order to verify this speculation.

In what follows, we describe the observation of a new twist grain boundary phase exhibited by a binary mixture. This structure is characterised by a *two-dimensional modulation of the grain boundaries* separating *smectic-C*-like blocks.* This structure is very different from the TGB_{C^*} structure predicted by Renn. The details of the experimental studies conducted on this new phase are described below.

4.2 Experimental studies

4.2.1 Materials used

The experimental studies were conducted on binary mixtures ccnsisting of the compounds 4-(2'-methyl butyl) phenyl 4'-n-octylbiphenyl -4-carboxylate ($CE8$) made by BDH and 2-cyano 4-heptylphenyl 4'-pentyl 4-biphenyl carboxylate ($7CN5$) obtained from Merck. The chemical structures of the two components are shown in Fig. 4.5. Note that the two components of the mixture have similar lengths and molecular weights.

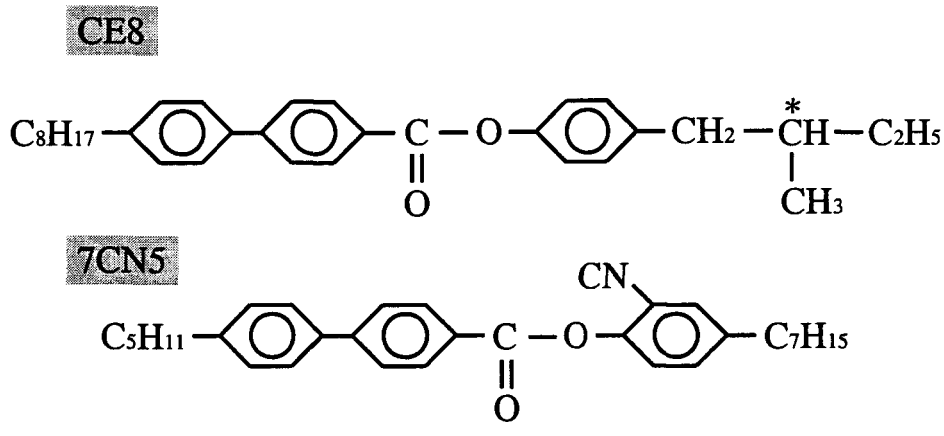

Figure 4.5: Molecular structures of the two compounds used in the experiments.

The first compound, $CE8$, is *chiral* due to the presence of the asymmetrically substituted carbon atom. It has the following phase sequence as a function of temperature (in ^oC): K – 67 – SmI^* – 70 – SmC^* – 85.0 – SmA – 134.6 – N* –

138.8 – BP2 – 139.7 – $BP1$ – 140.5 – I, where K denotes the crystalline phase and BP stands for the blue phases. All these phases, especially the SmC^* phase, have been well characterised [48, 49, 50]. The second compound, $7CN5$, does not have any chiral centers and hence is *achiral.* It shows a nematic phase over a very wide range of temperatures and has the phase sequence K – 45.5 – N – 102.0 – I (temperatures in ^oC). The nematic phase of this compound exhibits a strong *skew-cybotactic* [51, 1] (SmC-like) short range ordering in the entire temperature range [29], as was already discussed in Sec. 2.2. Moreover, the nematic easily supercools down to room temperatures ($\sim 28^oC$) though the crystal melts only at 45.5^oC.

The mixtures were prepared by weighing precise amounts of each component in a glass sample cup. The sample was then heated to the isotropic phase and mixed thoroughly using a thin glass rod. The mixture was then left in the isotropic phase for some time for it to attain a uniform concentration. The sample cells were filled with the sample in the isotropic phase. It was noticed that when the sample was left at a high temperature for a few hours, its composition changed due to a preferential evaporation of $7CN5$. To avoid such complications, the sample cells were sealed using a silicon based glue whenever an experiment had to be done over a long period of time.

4.2.2 Textural studies and phase diagram

One of the simplest and most inexpensive methods of identifying and studying the various liquid crystalline phases is by observing their 'textures' using a polarising microscope [26]. Each liquid crystalline phase exhibits its own characteristic texture which can betray the symmetry of the underlying structure.

The microscopic observations were made using a Leitz polarising microscope. The sample was taken between a slide and a cover-slip. The temperature of the sample was controlled using a Mettler FP80 hot-stage with an accuracy of 0.1^oC.

In pure $CE8$, between crossed polarisers, the higher temperature blue phase appeared with a characteristic mosaic texture with colours varying from deep purple to light green. On cooling the sample there was a transition to another blue phase during which the colour suddenly changed to reddish brown. The transition to the cholesteric phase was marked by the appearance of a bright schlieren texture. On cooling to the smectic-A phase, the sample spontaneously aligned with the smectic layers parallel to the plates (homeotropic alignment) and hence appeared perfectly dark. In the smectic-C* phase, the texture became slightly greyish (pseudo-homeotropic) due to the tilting of the molecules with respect to the layer normal.

In mixtures having about $5wt\%$ to $33wt\%$ of $7CN5$, a TGB phase intervened between the cholesteric and the SmA phases. The N*$-TGB$ transition was difficult to detect, but a gentle displacement of the cover-slip produced slightly different textures in the cholesteric and the TGB phases. When cooled from the isotropic phase without disturbing the cover-slip, the TGB pitch lines were clearly visible. The pitch lines are the optical patterns produced by the twisted arrangement of the director when the twist axis is parallel to the plane of the slide. This is best seen when the sample is viewed between crossed polariser and analyser. On cooling to the SmA phase, the sample aligned homeotropically. On reheating a filamentary growth, characteristic of the TGB phases [52], was observed. Since this phase occurred between the N* and the SmA phases, it was identified as the TGB_A phase. This was later confirmed by xray experiments.

In a mixture with about $33wt\%$ to $40wt\%$ of $7CN5$, a new texture appeared when cooled further from the TGB_A phase. In this, the pitch-lines of the TGB_A phase became corrugated with a well defined periodicity. Also, small patches showed a square lattice modulation. The texture appeared grainy compared to that of the TGB_A phase. At a lower temperature most of the sample aligned pseudo-

homeotropically. On reheating, flower-like patches and corrugated filaments grew in the pseudo-homeotropic regions. Above a well defined temperature the filaments became smooth like those of the TGB_A phase. In a mixture with more than about $42wt\%$ of $7CN5$, the grainy texture with patches of square lattice appeared immediately below the cholesteric phase. The detailed phase diagram of the mixtures constructed by textural observations is shown in Fig. 4.6.

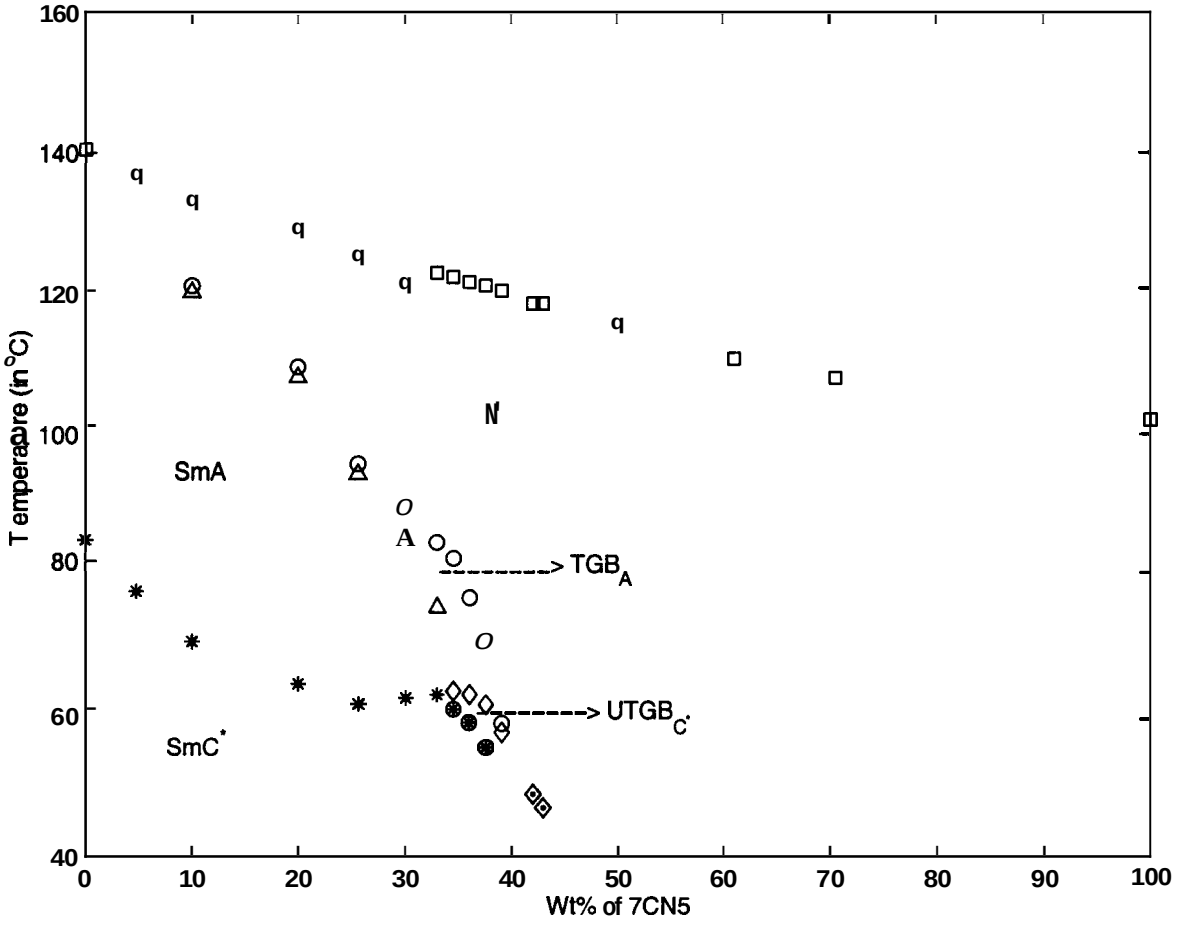

Figure 4.6: Phase diagram for the $CE8$-$7CN5$ mixtures. The region where the new phase occurs is marked as $UTGB_{C^*}$ for reasons explained later in the text. The transitions between different phases are shown using different symbols.

Thus, although pure $CE8$ does not show any TGB phases, the addition of as small as $5wt\%$ of $7CN5$ induces a TGB_A phase. Above $\sim 33wt\%$ of $7CN5$ there is a transition from the TGB_A phase to a new phase which has a very different texture

from those already known. At still higher concentrations of $7CN5$ the new phase occurs immediately below the cholesteric phase. Beyond $\sim 43wt\%$ the cholesteric phase extends down to room temperature. All the transitions were sharp and *no measurable coexistence* was seen. It is interesting to note that the addition of an achiral compound stabilises the TGB phases in a very wide concentration range. In the case of TGB_A, this trend has been reported in several binary mixtures of chiral and achiral compounds [46, 53].

In order to further characterise the new phase, several experiments were conducted using sample cells treated for specific alignment of the director. All the experiments described 'below were conducted using mixtures with about $36wt\%$ of $7CN5$. This mixture showed the following phase sequence as a function of temperature: $K-SmC^*-59.0-X-63.0-TGB_A-76.8-N^*-121.2$–BP2–121.5–BPI–121.7–1, where X denotes the range with the new texture. Since fresh mixtures were made for each experiment, there were small variations (about 0.3%) in the sample composition from one experiment to another. The slight discrepancy in the transition temperatures in different experiments described in the later sections mainly arises due to this reason.

4.2.3 Differential Scanning Calorimetric studies

In order to study the nature of the phase transitions between the various phases, we conducted differential scanning calorimetric (DSC) studies using a Perkin Elmer DSC7 (Pyrisl) calorimeter. About 29mg of the mixture was weighed into the sample cup and mixed thoroughly after heating to the isotropic phase. With such a large quantity of sample, which was necessary to detect some of the weaker transitions, it was not possible to crimp-seal the cups. This limited the amount of time the sample could be kept at high temperatures without it undergoing degradation or changes in the composition. The temperature was ramped at a fairly large rate of $10^oC/min$ to improve the signal level. This, of course, reduced the resolution. For example,

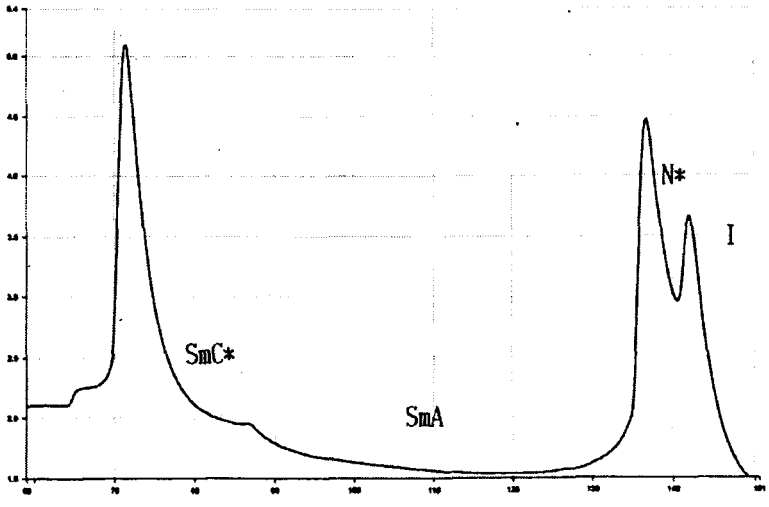

Figure 4.7: The DSC scan of pure CE8. The closely spaced blue phases are not resolved. The $SmA - SmC^*$ transition is second-order.

---

in the case of the mixtures as well as the pure CE8, the closely spaced blue phases could not be resolved. The other interesting transitions were not affected as they were widely spaced along the temperature axis. The sample temperature was cycled a few times starting from the isotropic phase before collecting the data. In the case of the mixtures several cooling runs were added to produce the curves shown in Figs. 4.7 to 4.11.

In the case of pure CE8, all the transitions, except those involving blue phases, were clearly visible (Fig. 4.7). The blue phases could be resolved at slower rates (1°/min). The $SmA - SmC^*$ transition is second-order in nature.

In the case of the mixtures, the N*–TGB_A–SmA transition temperatures were covered by a single broad peak. The individual transitions could not be resolved even at slow rates ($\sim 1^o/min$). Furthermore, this peak became broader as the concentration of $7CN5$ was increased (Figs. 4.8 to 4.10). It should be mentioned that such broad peaks for the $N^* - TGB_A - SmA$ sequence have been reported even for pure compounds [54, 55]. It is believed that the broad peak is due to the

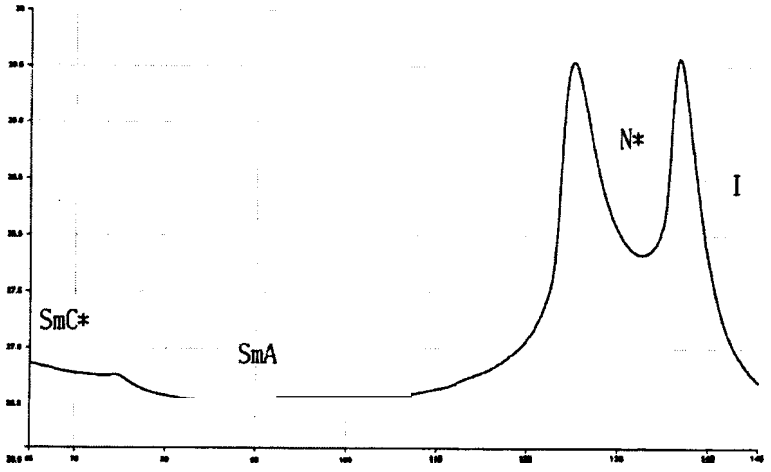

Figure 4.8: The DSC scan of a mixture with $10.2wt\%$ of $7CN5$.

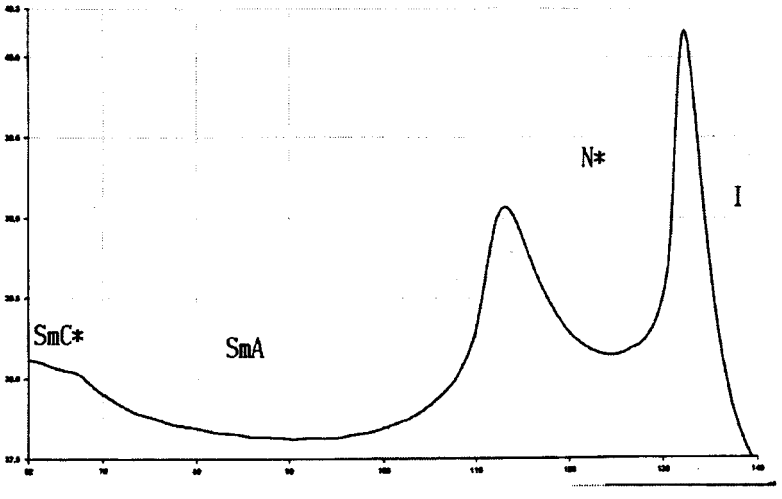

Figure 4.9: The DSC scan of a mixture with $19.8wt\%$ of $7CN5$.

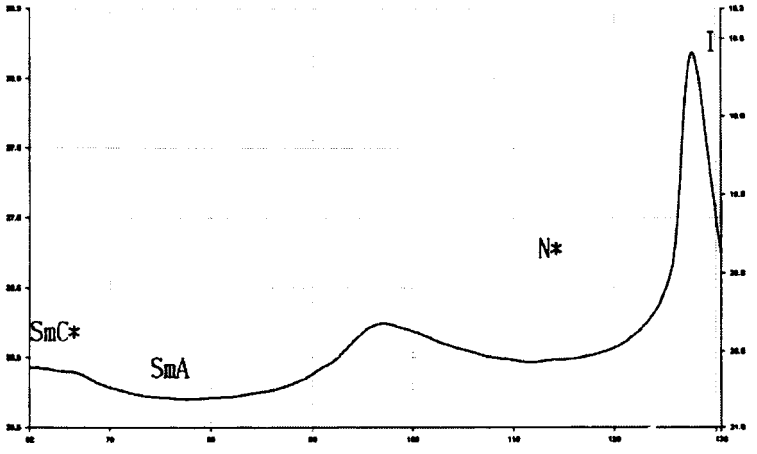

Figure 4.10: The DSC scan of a mixture with $29.8wt\%$ of $7CN5$.

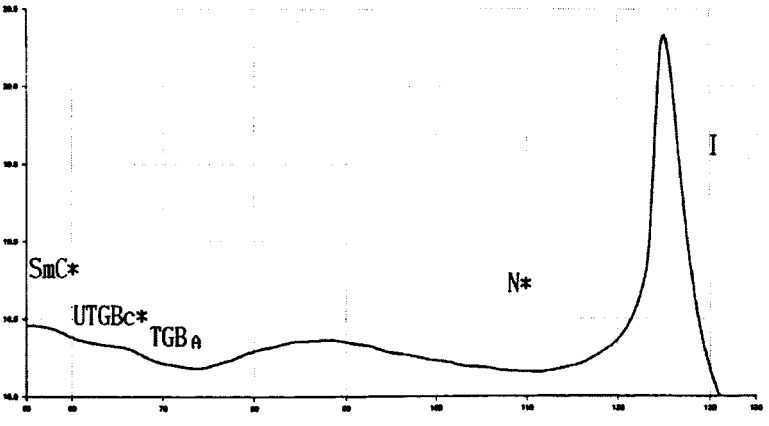

Figure 4.11: The DSC scan of a mixture with $34.5wt\%$ of $7CN5$. The $TGB_A - UTGB_{C^*}$ and the $UTGB_{C^*} - SmC^*$ transitions are seen as slope changes.

formation of a TGB-like short range order in the cholesteric phase. High resolution *a.c* calorimetric studies [54] show slight slope changes superimposed on the broad peak indicating transitions from the cholesteric with TGB-like short range order to the TGB_A phase and from the TGB_A to the SmA phase. Such a state with a TGB-like short range order is referred to as a chiral line liquid and is analogous to the Abrikosov vortex liquid in type-I1 superconductors [56].

For the mixture with $34.5wt\%$ of 7CN5, the transition from the TGB_A to the new phase and that from this phase to the SmC^* phase are clearly visible (Fig. 4.11). Both these transitions appear to be second-order.

4.2.4 Observations on cells treated for planar alignment

The director can be made to lie in the plane of the cell by an appropriate treatment of the glass surfaces of the cell. For this, the plates were spin-coated with a thin uniform layer of a polymer (Polyimide) solution. The plates were then cured at 300°C. After curing, the plates were unidirectionally rubbed using good quality tissue paper. This forces the director at the glass surfaces to lie along the rubbing direction. The cells were then constructed using mylar strips as spacers. The cell thickness was typically about $15\mu m$.

In cells treated for planar alignment, the TGB_A phase exhibited a Grandjean-plane texture [9] similar to that shown by the cholesteric phase. In such samples the boundary conditions ensure that the twist axis is perpendicular to the glass plates. Also, as the director alignment is fixed on the glass surfaces, only an integral number of half pitches can be accommodated between the plates. This is because the effective periodicity is half the TGB pitch due to the $\hat{\mathbf{n}} \equiv -$fi symmetry. The local changes in the cell thickness produces sympathetic variations in the helical pitch, producing the Grandjean-plane texture. This is best seen in wedge shaped cells constructed by using a spacer only at one edge of the cell (Fig. 4.12). The number

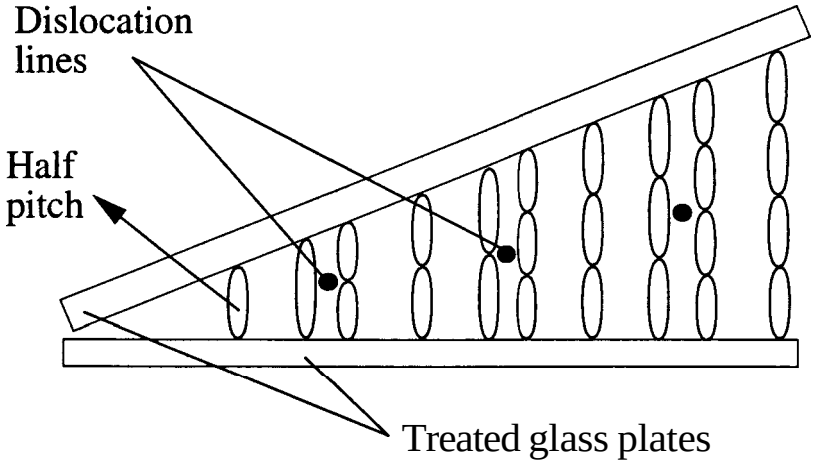

Figure 4.12: A schematic representation of the cholesteric/TGB structure in a wedge shaped cell treated for planar alignment. The number of half pitches jumps by integer values across each dislocation line. The pitch gets compressed/dilated close to the dislocaiion lines as shown.

---

of half pitches jumps by integer values across each Grandjean-Cano (GC) dislocation line [1]. Thus, the GC dislocation lines can be considered as edge dislocations in the cholesteric or TGB periodicity. In uniformly spaced cells, as the temperature is lowered to below 63.0°C, the texture changes over to a well aligned square *grid* pattern, one of the axes of which is, on the average, parallel to the rubbing direction.

In wedge shaped cells, in which the cell thickness varied continuously from one edge of the cell to the other, an array of equidistant GC lines formed in the TGB_A as well as in the cholesteric phase (see Fig. 4.13a). In between the lines the texture was very smooth with a gradual colour variation from the thinner to the thicker side of the cell. The colour variation was due to the changes in the helical pitch induced by the treated glass plates. As the temperature was lowered(increased) the spacing between the lines increased(decreased), indicating that the pitch of the structure was increasing(decreasing). On cooling to below 63.0°C, the square grid appeared to start from the thinner side of each GC line and filled the entire region within 0.1^oC. A photograph of the square grid texture taken using a wedge shaped cell is shown in Fig. 4.13b. The array of straight GC lines continued to exist and

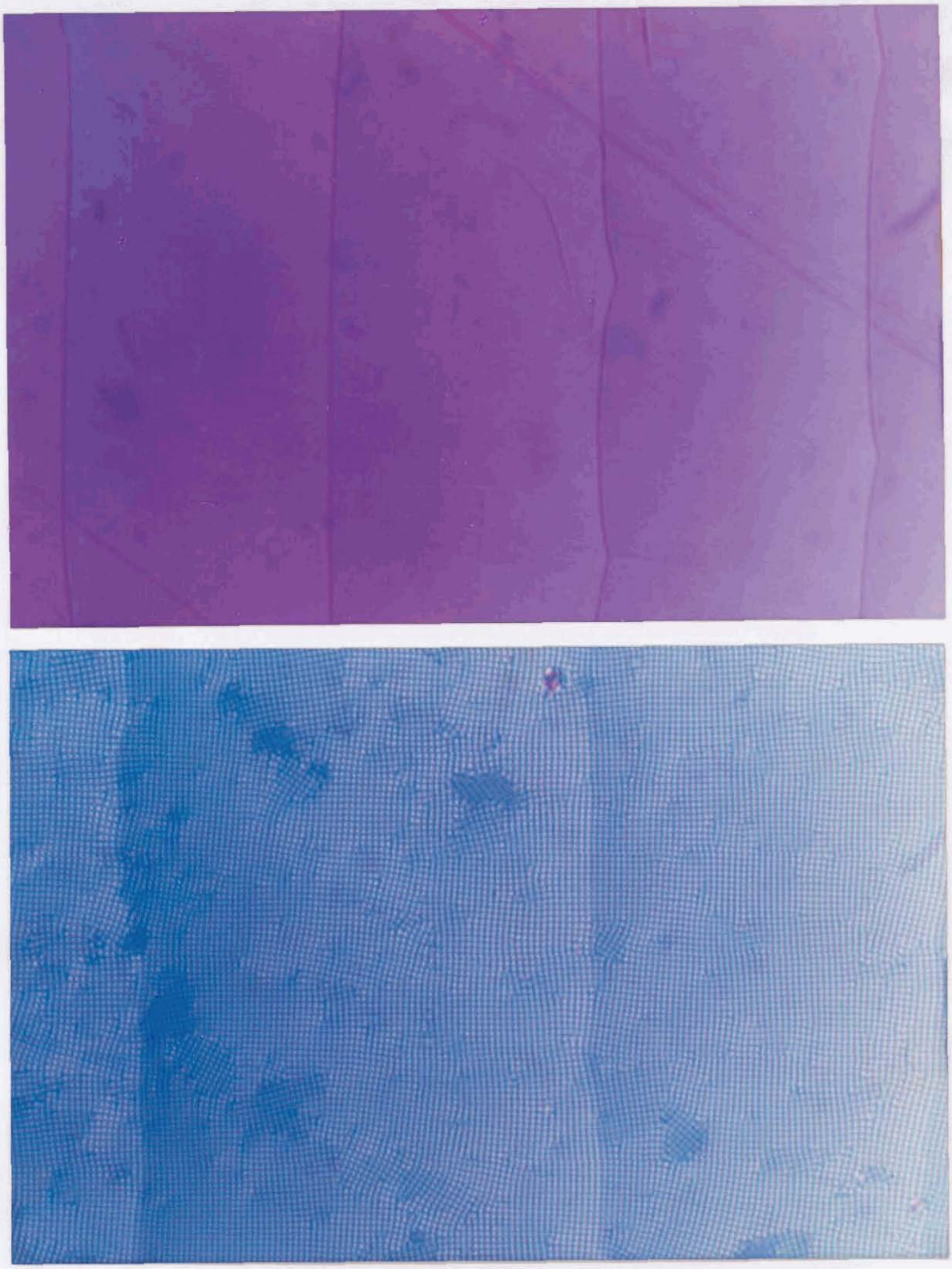

Figure 4.13: (a) Photograph of the TGB_A texture in a wedge shaped cell. The vertical lines are the *GC* lines, which indicate that there is a twist deformation in the director along the normal to the glass plates, *ie.* along the viewing direction. (b) The same region, recorded after the transition to the square grid texture was complete. The grid spacing is anout $2\mu m$. The *GC* lines are clearly visible. The increase in the spacing between the *GC* lines compared to the TGB_A case shows that the pitch of the structure is larger than that of the TGB_A. The colour variation is also due to this reason.

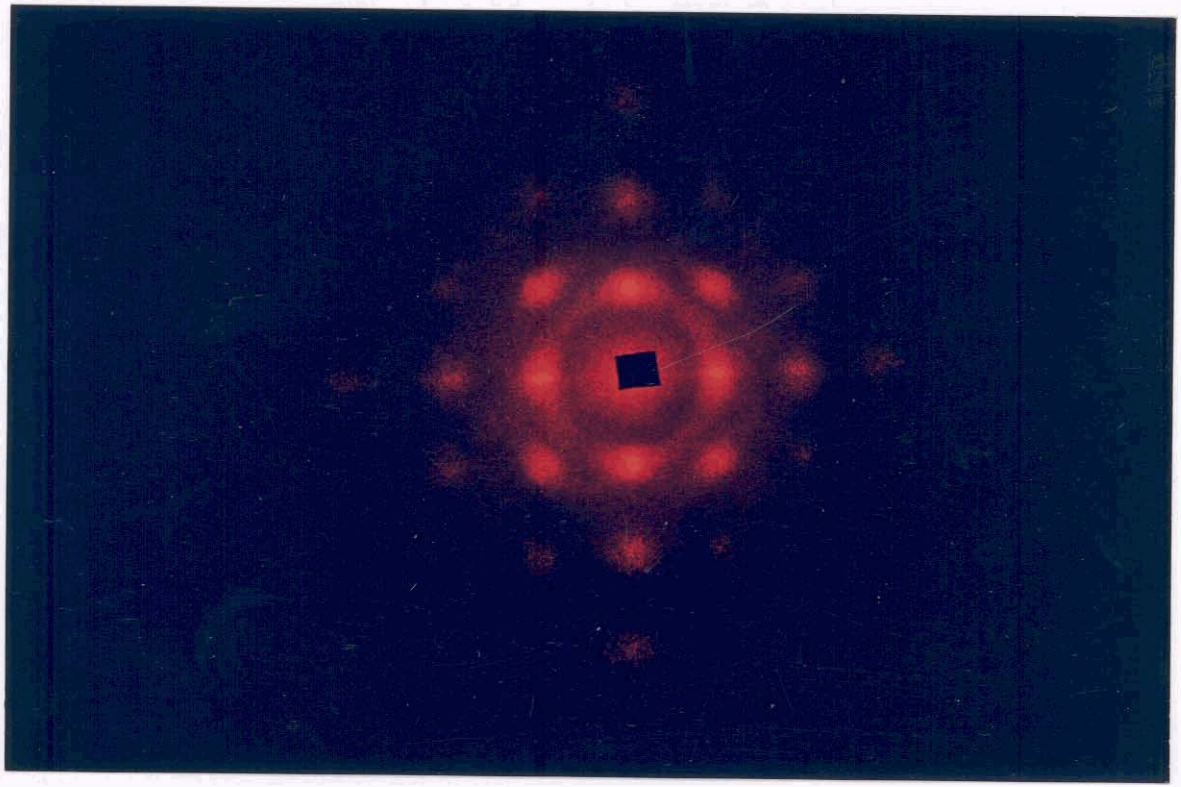

Figure 4.14: The diffraction pattern obtained by shining a *He-Ne* laser beam on a planar aligned wedge shaped sample with square grid texture. The beam was incident normal to the cell.

the spacing between them continued to increase(decrease) as the temperature was reduced(increased) to 59.0^oC. Below 59.0^oC, the GC lines suddenly became highly distorted and non-periodic. Moreover, the lines did not shift with the lowering of the temperature. The square grid, however, remained visible though the contrast deteriorated a little and coloured patches appeared in the background. When the temperature was increased, the original square grid texture was recovered at 59.0^oC within about $5min$, as were the distinct and straight GC lines in the wedge shaped cells. The presence of the GC lines along with the square grid between 63.0°C and 59.0°C indicates that the structure in this temperature range is 'twisted' with the twist axis normal to the glass plates as in the TGB_A and the N^* phases.

The optical diffraction pattern obtained by shining a *He-Ne* laser beam on a well aligned sample with the square grid structure is shown in Fig. 4.14. The wedge shaped cell was chosen as it gave better alignment of the square grid. In the TGB_A phase no pattern was observed. The transition to the new phase was marked by the appearance of a pattern with many orders of diffraction maxima. The pattern revealed the underlying two-dimensional modulation of the effective refractive index. The pattern continued to exist below 59.0°C.

In order to confirm that the square grid pattern was not due to any surface effects, the above experiments were repeated using **glycerine coated cells.** For this the glass plates were smeared with a thin, uniform, layer of glycerine before assembling the cell. Glycerine is immiscible with the liquid crystal and this was confirmed by verifying the transition temperatures. At the liquid crystal-glycerine interface the director prefers to lie parallel to the interface, but no particular azimuthal direction is preferred. In such cells, the TGB_A phase showed a Grandjean plane texture as before. Below the TGB_A phase, the square grid texture appeared, but with several randomly oriented domains. The transition to the SmC^* phase was more pronounced, with the appearance of patches of different colours, though

again the square grid pattern remained. In the SmC^* phase (below 59.0°C) a slight displacement of the top plate removed the grid completely. On holding the temperature constant for a few hours, a focal-conic texture characteristic of the SmC^* phase [26] developed in some regions. On slowly increasing the temperature to 59.5^oC, the square grid texture started reappearing within about $10min$ and filled the entire sample area within an hour. This proved that that the square grid texture below this temperature was due to a *pseudomorphotic* (metastable) structure. When the top plate was displaced, with the sample in the intermediate phase ($\sim 59.5^oC$), the square grid reappeared within a few minutes. Of course, in a wedge shaped cell with glycerine coated plates, no GC lines formed due to the degeneracy in the boundary condition and the lattice spacing of the square grid was found to be *independent* of the thickness of the cell. Furthermore, the square grid appeared everywhere simultaneously. If the square grid texture was a result of some kind of strain-induced instability of the kind seen in usual smectics or cholesterics [1, 2], the lattice spacing as well as the threshold value of the strain for the instability to occur should have shown a dependence on the thickness of the cell, since the amount of strain developed depends on the thickness of the sample. Also, such instabilities are usually observed only when the temperature is *either* increased or decreased and *not* in both runs.

4.2.5 Observations on cells treated for homeotropic alignment

In order to favour **homeotropic alignment** (Frank-director normal to the glass plates), the glass plates were coated with a monolayer of octadecyl triethoxy silane (ODSE) by dipping the plates in a dilute solution of the surfactant. The plates were then cured at 150^oC for one hour. Cells were constructed using $10\mu m$ thick mylar strips as spacers. The sample, a mixture with $36.0wt\%$ of $7CN5$, was filled in the cell when it was in the isotropic phase by capillary action. On cooling to below 59.0°C, good pseudo-homeotropically aligned SmC^* was obtained. In this, the smectic lay-

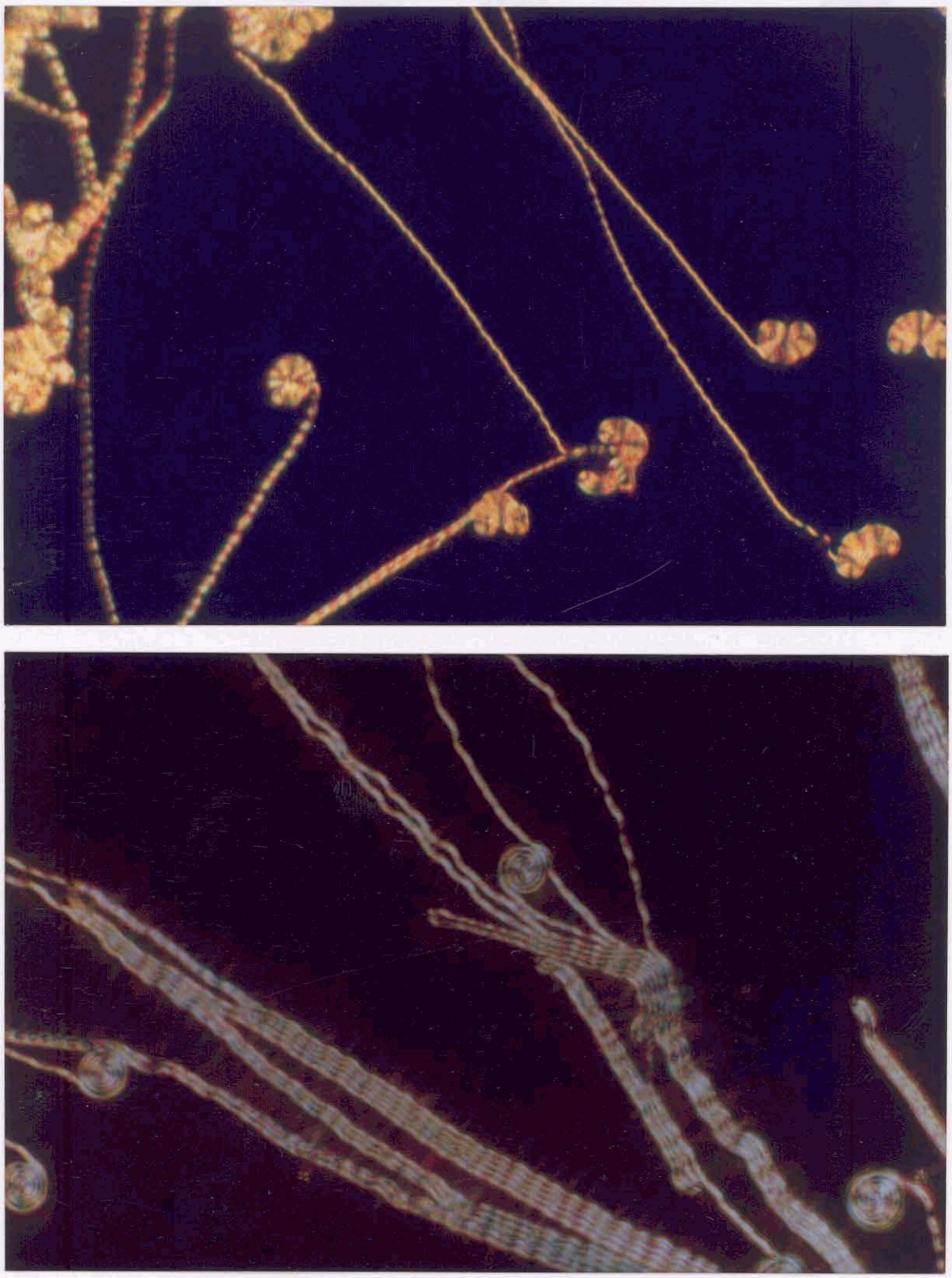

Figure 4.15: Photographs of the corrugated filaments. When many filaments form side by side the corrugations in them are in phase. Each filament corresponds to half a TGB pitch. The lines separating adjacent filaments are in fact the pitch-lines of the TGB. The width of each filament is approximately $1.5\mu m$.

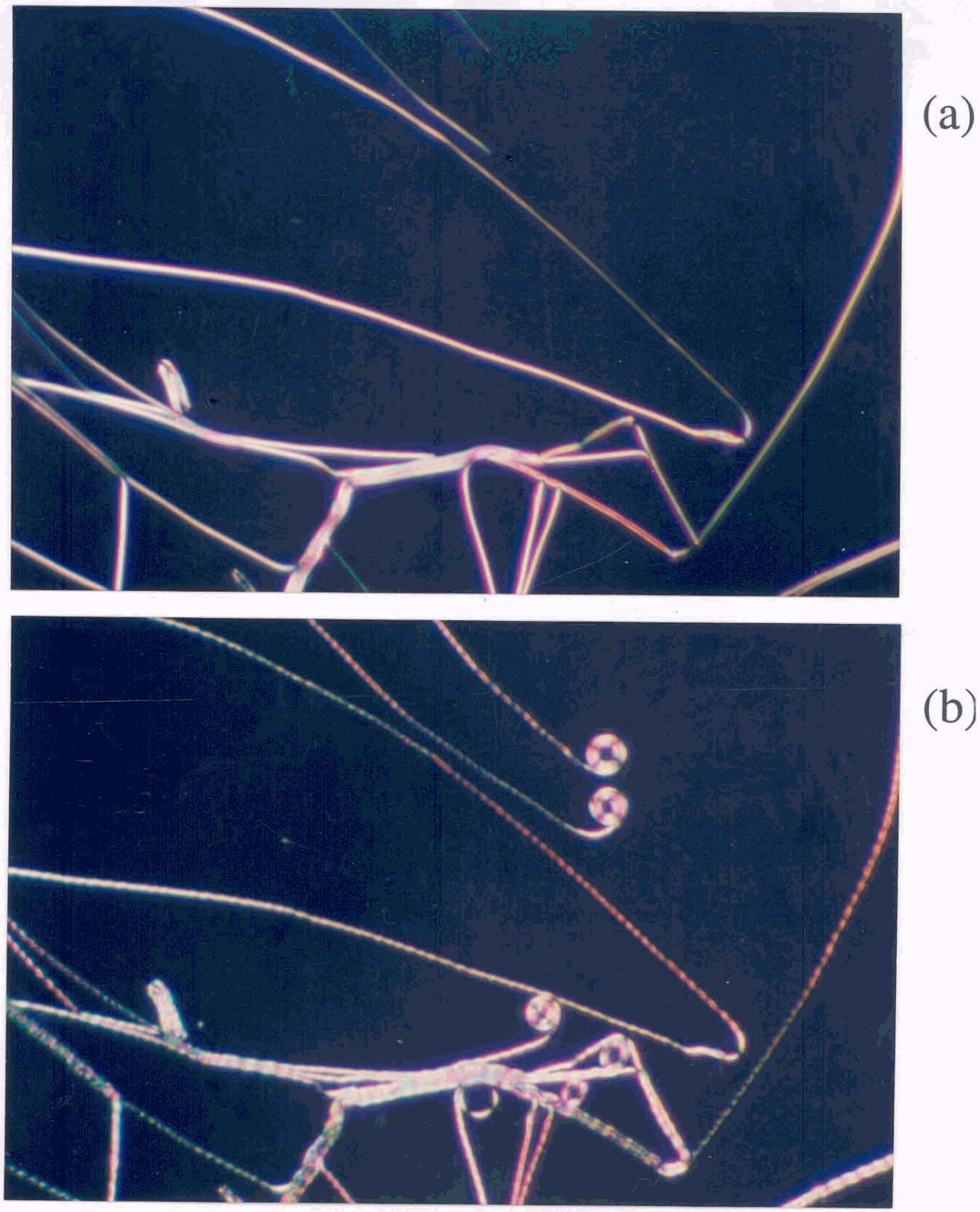

Figure 4.16: The filamentary texture in the (a) TGB_A phase and (b) in the new phase. The smooth filaments of the TGB_A phase becomes corrugated when cooled to the new phase.

ers are arranged parallel to the glass walls of the cell. As the SmC^* pitch was small in this case, the sample appeared almost completely dark between crossed polarisers. On slowly heating the sample from this state, bright filaments started growing against the dark background. Mostly they grew as corrugated spirals. Sometimes, especially on fast heating ($\sim 1^oC/min$), they formed loose periodically corrugated filaments (see Figs. 4.15a,b). Above 63.0°C the periodic corrugations of the existing filaments smoothened out and new filaments which developed were all smooth and almost straight (see Fig. 4.16a). The straight smooth filaments are typical of the TGB_A phase [52]. The width of the filaments corresponds to half a TGB pitch (a rotation of the F'rank-director by π radians). This is easy to verify as they can be completely crossed out by setting one of the polarisers along the filament axis and the other in the crossed position. This is because in such a structure the projection of the Frank-director is everywhere parallel to the filament and hence does not affect the state of polarisation when the incident polarisation is either parallel or perpendicular to the filaments. When the sample was cooled to below 63.0°C, all the filaments again started developing corrugations (see Fig. 4.16b). Also, the tips of the filaments, which continued to grow, started spiraling. Now, when the polariser was rotated in either direction with respect to a filament, only alternating regions which were parallel to the polariser appeared as dark patches. The bright portions appeared as patches with the maximum brightness at the middle of the filament. This means that the Frank-director (or its projection) is more or less parallel to the local filament orientation near the middle part of the filaments. As the temperature was lowered further, the corrugations became more pronounced and the wave length of the corrugations decreased. Below 59.0^oC, these filaments shrank and disappeared to produce the pseudo-homeotropic texture of the SmC^* phase. Note that above 59.0°C the SmC^* structure, which appeared dark, was metastable and when the temperature was held constant for several minutes the filaments filled

the entire sample area.

In **open drops** of the sample deposited on a glass plate treated for homeotropic alignment, concentric Grandjean-Cano lines were clearly visible in the SmC^* phase. This was due to the SmC^* helix whose axis was along the normal to the glass plates. On heating to 59.0^oC, corrugated filaments grew in concentric arcs. The GC lines *remained* till close to 63.0^oC. The spacing between the GC lines did not show any appreciable variation with temperature indicating that the SmC^* pitch remained more or less constant. Above 63.0°C, the filaments became smooth but continued to grow in arcs and the remaining portion of the sample was perfectly homeotropic without any GC lines. Apart from confirming the SmC^* structure below 59.0^oC, this experiment also indicated that the smectic tilt angle was non-zero between 59.0^oC and 63.0^oC and was zero above this temperature range. This means that the TGB structure above 63.0^oC was indeed TGB_A and below this was a TGB structure with a tilt order within the smectic layers. This was also confirmed by xray diffraction experiments described in a later section. However, the corrugated appearance of the filaments in the new phase was strikingly different from those formed by materials exhibiting the usual TGB_C phase, where the smooth filamentary texture is indistinguishable from that of TGB_A.

The above microscopic observations show that the new texture corresponds to a *thermodynamically stable* phase which appears both on cooling from the TGB_A phase and on heating from the SmC^* phase. The presence of the Grandjean-Cano lines along with the square grid in wedge shaped cells and the filamentary growth exhibited in the homeotropic cells strongly suggest that this structure is due to a *new twist grain boundary phase.*

The undulating structure of the filaments in the homeotropic case and the corrugated pitch-lines in the untreated cells suggest that the grain boundaries separating the smectic blocks are also undulatory. The pitch lines are formed by a continuous

repetition of the filament structure and can be viewed as a tight packing of the filaments. In these two cases the TGB twist axis was in the plane of the cell and perpendicular to the viewing direction, whereas, in the case of planar alignment it was perpendicular to the glass plates and hence along the viewing direction. The filaments are, therefore, a 'side view' of the square grid structure seen in the planar aligned cells. This is also supported by the fact that the periodicity of the filament undulation is very much comparable to the lattice spacing of the square grid. Furthermore, the variations of the filament wave-length and the lattice spacing of the square grid with ternperature show similar trends. Based on these facts we propose that the grain boundaries separating the smectic blocks of this phase have a *two*-dimensionally undulating character. Thus, unlike the TGB_A or the TGB_C phases this new phase has a structure which is three-dimensionally modulated. This point will be discussed again towards the end of this chapter.

4.2.6 Pitch and lattice spacing measurements

The pitch corresponding to the various twisted phases was measured as a function of temperature from the spacing between the GC lines in the wedge shaped cell. The sample was cooled to the required temperature at $0.1^oC/min$ and held at that temperature for a few minutes (till the GC lines became stationary) before making each measurement. The spacing between the GC lines was measured using a graduated eye-piece with a least count of $\sim 3\mu m$, which was calibrated using a micrometer scale provided by Leitz. The wedge-angle of the cell was $0^o14'52''$. The angle was measured using a goniometer which has a least count of 2''. The pitch value was calculated using the formula $\tan\theta = p/2l$, where θ is the wedge-angle, p is the pitch and 1 is the spacing between the GC lines. Note that the factor of $1/2$ comes because the relevant periodicity is half the pitch, ie. a rotation of the director by π radians. It was seen that the pitch increased smoothly from the N* to the TGB_A phase (Fig. 4.17). The transition to the square-grid structure was observed at 62.5^oC.

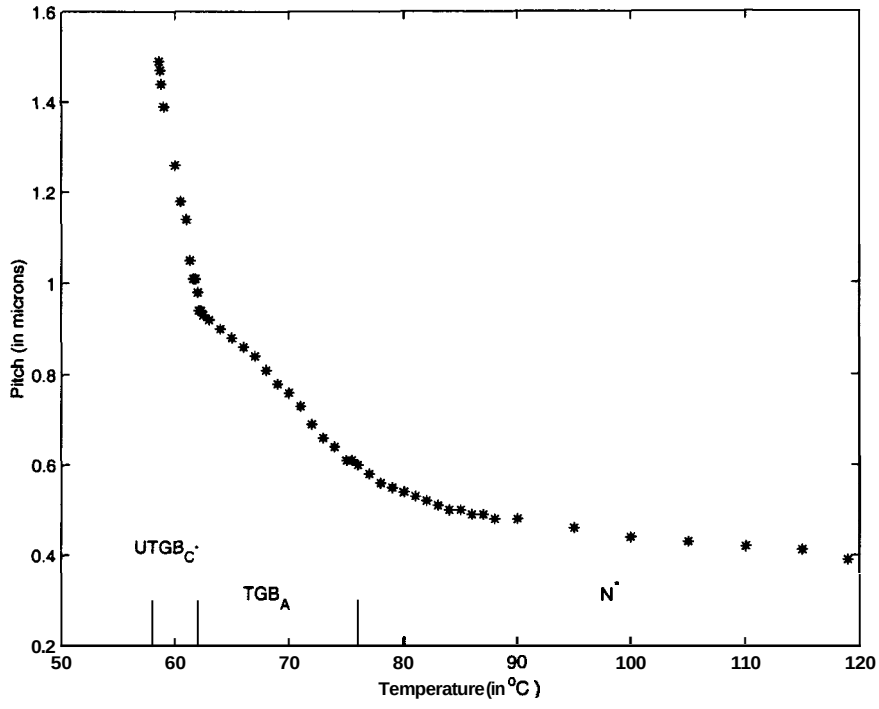

Figure 4.17: Variation of the pitch as a function of temperature in the various twisted phases. The transition temperatures are indicated by vertical lines.

Below this temperature, the pitch increased very sharply till 58.6^oC. The slope of the curve was *discontinuous* at 62.5^oC though the pitch changed *continuously* across this temperature. The variation of the pitch with temperature was very similar to that observed by the Bourdeaux group in compounds showing a TGB_C phase [57] (see Fig. 4.18).

The pitch of the SmC^* phase below 59.0°C was also measured using a wedge shaped cell whose plates were coated with ODSE and very gently rubbed to align the c-vector at the plates. A good alignment, with the smectic layers parallel to one of the plates, was obtained by gently pressing the top glass plate. The spacing between the GC lines and hence the SmC^* pitch did not show any appreciable variation with temperature. In the thinner most part of the wedge the $SmC^* -$ TGB transition temperature was higher ($\sim 1^oC$) compared to that at the thickest end. Thus, the pitch of the metastable SmC^* could be measured up to a couple of degrees above the $SmC^* -$ TGB transition temperature. Beyond this the GC lines became too

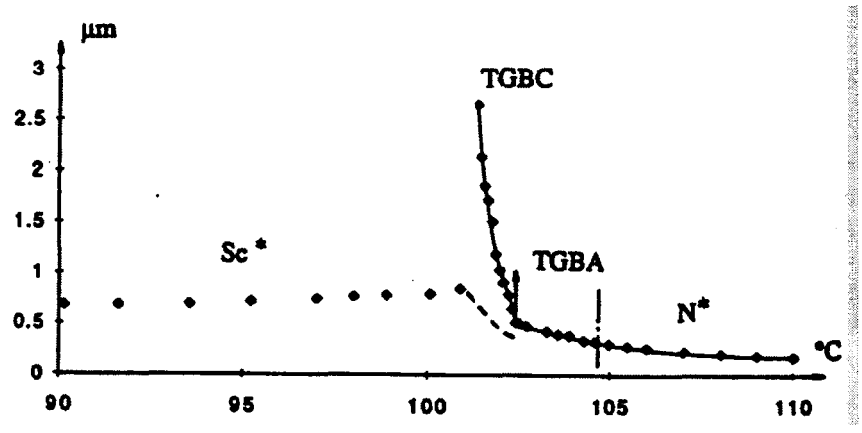

Figure *4.18:* The variations in the pitch in a compound showing $N^* - TGB_A - TGB_C - SmC^*$ sequence (reproduced from Ref. [57]. The variations are similar to that shown in Fig. *4.17.*

---

faint to allow any measurements. The SmC^* pitch had an almost constant value of $1.4\mu m$ in the entire range of temperatures where measurements could be made. The SmC^* pitch reported for pure $CE8$, however, decreases from $2.8\mu m$ at 80^oC to about $1.6\mu m$ at 71^oC [49].

The lattice spacing of the square modulation was also measured as a function of temperature. The measurements were made using a cell treated for planar alignment. Though both the plates were coated with polyimide, only one of them was rubbed in order to reduce effects due to surface anchoring. The cell thickness was $23\mu m$. The lattice spacing was measured from the diffraction patterns obtained by shining a $He\text{-}Ne$ $(632.8nm)$ laser beam along the normal to the glass plates. The distance between the diffraction maxima was measured from a screen placed at a distance of $317mm$ from the sample. The maximum cooling rate was $0.1^oC/min$ and the temperature was held constant for about $5min$ before making each measure-

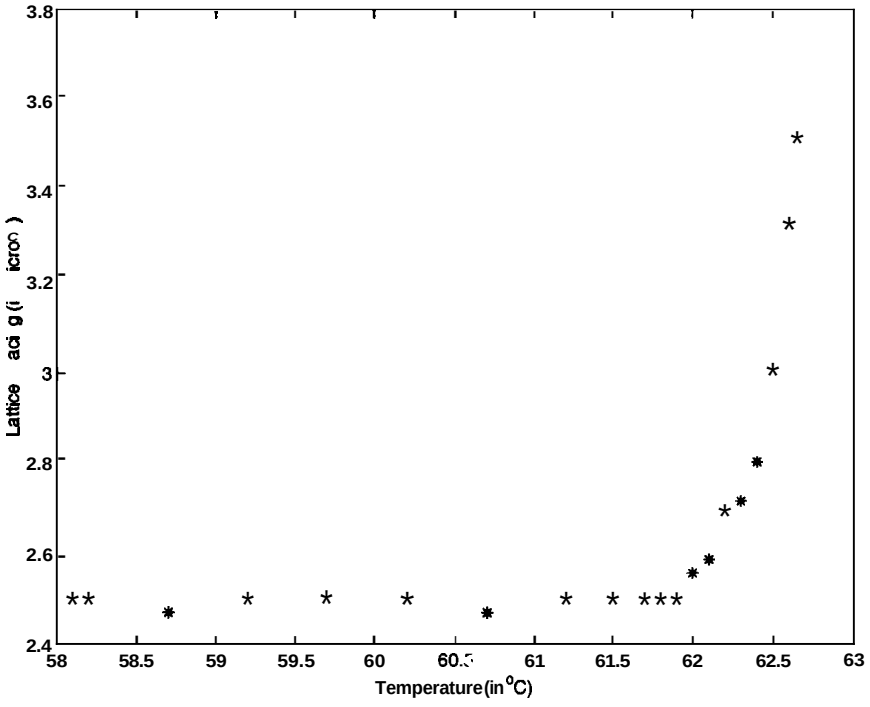

Figure *4.19:* Variation of the lattice spacing of the square modulation as a function of temperature. The measurements were made by cooling the sample from the TGB_A phase.

---

ment. The variation of the lattice spacing with temperature obtained while cooling is shown in Fig. *4.19.* Under the microscope the TGB_A to square grid transition was observed at 62.7^oC. The spacing dropped sharply just below the transition from the TGB_A phase and leveled off at around 1.5^oC below the transition temperature. When the sample was heated at the same rate, the lattice spacing variation was faster compared to that obtained on cooling. However, when glycerine coated plates were used, both the cooling and heating runs produced curves similar to Fig. *4.19.* Therefore, the discrepancy observed in the first case might have been due to surface effects.

4.2.7 Xray diffraction studies

Xray diffraction studies were carried out on aligned as well as powder samples.

In the case of **powder samples,** the sample was taken in a $0.5mm$ diameter Lindemann capillary tube. The sample was filled in the isotropic phase and the

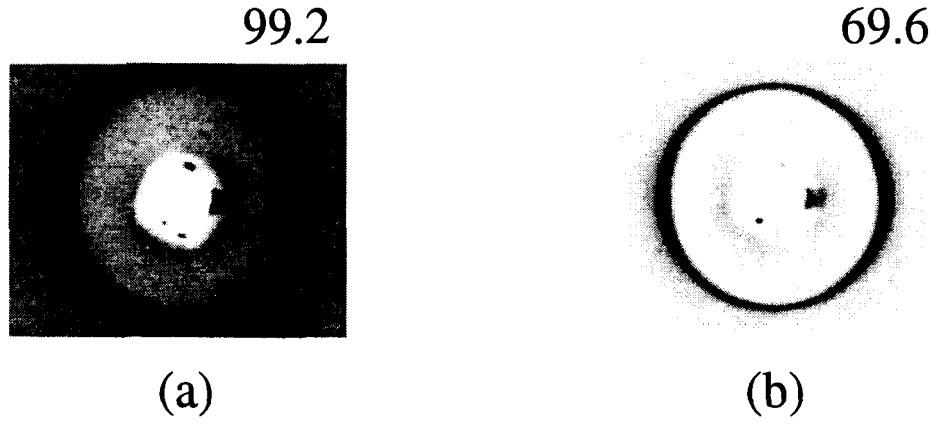

Figure 4.20: The xray diffraction patterns obtained from powder samples. (a) Well within the cholesteric phase (99.2^oC) after an exposure of $70min$. (b) Well within the TGB_A phase (69.6^oC) after an exposure of $15min$. The oven was equipped with a pair of permanent magnets. The higher intensities along the horizontal direction arises from the aligning effect of the magnetic field. The director prefers to align parallel to the field and hence the twist distortion in the N* and the TGB structures becomes nonuniform.

---

ends of the capillary were flame-sealed. The sample was mounted in a computer controlled oven which had an accuracy of $\pm 10mK$ (Sec. 2.4). The xray beam from a Rigaku 18kW rotating anode xray generator was first filtered using a $15\mu m$ thick Ni foil and then collimated using a double-slit arrangement. The collimated beam had a cross-section of roughly 0.5 x $0.5mm$ at the sample. The scattered intensity was recorded on an image plate with an effective pixel size of $100\mu m$, procured from Marresearch. The sample to detector distance was $202.5mm$. A schematic diagram of the xray diffraction set-up is shown in Sec. 2.2.5.

The sample was first heated to the isotropic phase and the temperature was maintained constant for about $20min$. The diffraction patterns were recorded on cooling, starting from the cholesteric down to the SmC^* phase. The exposure time was varied from $120min$ at the highest temperatures to about $15min$ in the SmC^* phase. Well within the cholesteric phase, a uniform ring with a rather broad radial intensity distribution was obtained (Fig. 4.20a). The real space periodicity which produced this ring was roughly equal to the average of the molecular lengths of the

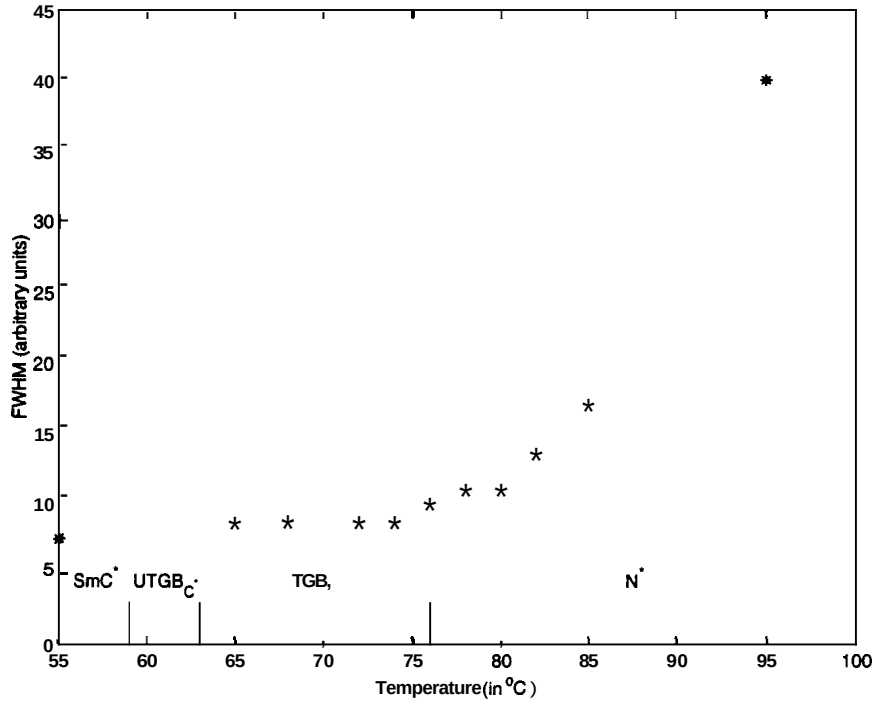

Figure 4.21: The Full Width at Half Maximum measured from the xray diffraction patterns obtained from powder samples. The peaks become resolution limited below $\sim 70^oC$. The transition temperatures measured from the textural observations are indicated by the vertical lines.

---

individual components of the binary mixture. On lowering the temperature to well within the TGB_A phase, the ring became very sharp compared to that obtained from the cholesteric phase (Fig. 4.20b). Within the limitations of the instrumental resolution, no coexistence of N* and TGB_A phases was seen. The temperature dependence of the full width at half maximum (FWHM) of the peaks obtained after angular integration of the intensity distribution is shown in Fig. 4.21.

The FWHM decreases rapidly as the temperature is lowered in the cholesteric phase and levels off below $\sim 70^oC$ in the TGB_A phase. The $N^* - TGB_A$ transition temperature measured from the textural observations was $\sim 76^oC$. An interesting point to note is that the FWHM changes continuously across the $N^* - TGB_A$ transition. This is probably due to the formation of a TGB-like short range order (chiral line liquid order) in the cholesteric phase as was discussed in Sec. 4.2.3. A similar trend in the FWHM variation has been reported for a pure compound which

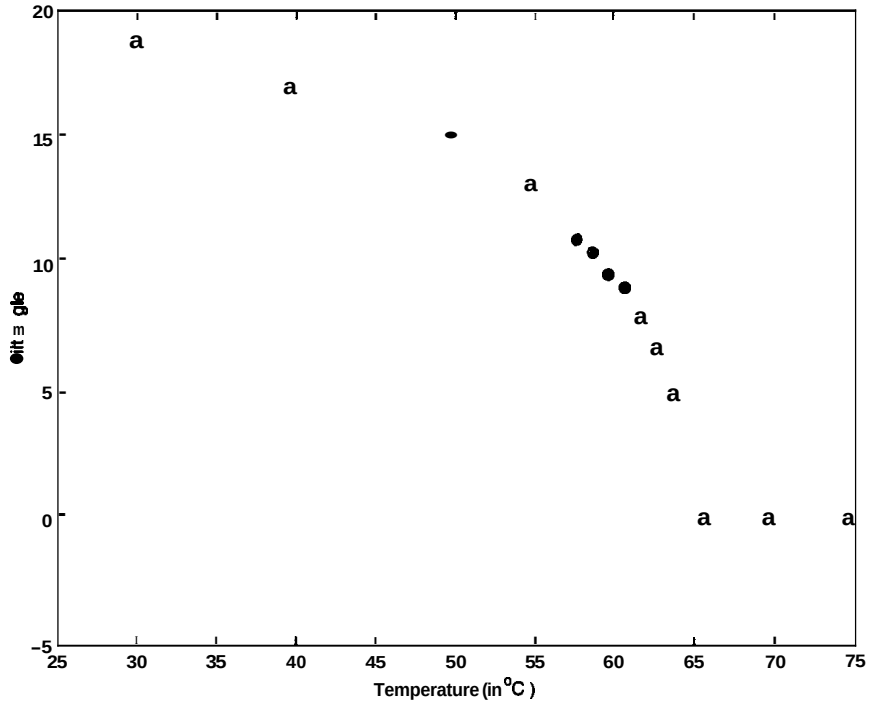

Figure 4.22: The variation of the smectic tilt angle calculated from the layer spacing measurements. The measurements were made on a mixture with about $34wt\%$ of $7CN5$.

---

shows a commensurate TGB_A phase [58]. In fact, the smooth variation of the pitch across the N*$-$ TGB_A transition point (see Fig. 4.17) also supports this possibility. Below $\sim 70^oC$, the peaks are resolution limited. These measurements were made on a mixture with $35.8wt\%$ of $7CN5$. We have also measured the smectic layer spacing as a function of temperature. This was made on a mixture with about $34wt\%$ of $7CN5$. The layer spacing variation shows that the spacing has a constant value of $29.7\mathring{A}$ throughout the TGB_A phase. Below 64^oC the layer spacing starts decreasing indicating that the molecules are now tilted with respect to the layer normal. The tilt angle variation as a function of temperature is shown in Fig. 4.22. The tilt variation is very similar to that seen across a second-order $SmA-SmC$ transition.

Xray diffraction experiments were also performed on **aligned samples.** For this a cell was constructed using $30\mu m$ thick glass plates got by etching one side of each cover-slip (see Fig. 2.14a). The smooth surface was coated with SiO at an oblique angle by vapour deposition. Such a treatment favours a planar alignment

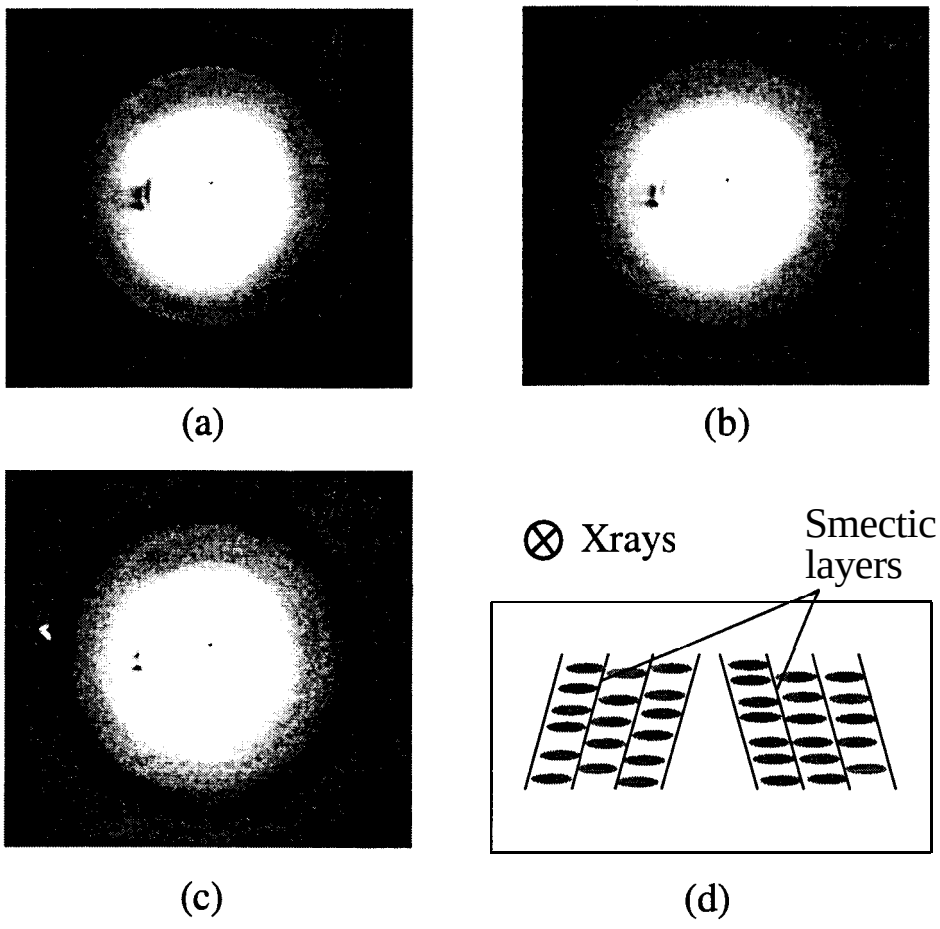

Figure *4.23:* The xray diffraction patterns obtained from the (a) TGB_A (b) $UTGB_{C^*}$ and (c) the SmC^* phases using a $25\mu m$ thick aligned sample. The temperatures (in ^oC) are indicated on the corresponding pictures. The exposure time was $120min$ in all the cases. (d) **A** schematic representation of two unwound domains of the SmC^* phase close to the glass plate. Such an arrangement of the layers can produce the intensity maxima seen in (c).

---

of the director at the coated surfaces [30]. The cell thickness was fixed at $\sim 25pm$ using mylar spacers. The cell was mounted in a Mettler $FP80$ hot-stage with mylar windows and the alignment was checked using an optical microscope before recording the xray diffraction patterns. The sample was illuminated by $Cu\text{-}K_\alpha$ radiation (selected using a Ni filter) from an Enraf fixed tube xray generator. The beam cross-section was about *2* x $2mm$. The diffraction patterns were recorded on the image plate. The exposure time given was *2* hours.

The diffraction from the TGB_A phase produced a continuous and relatively sharp ring compared to that obtained in the cholesteric phase (Fig. 4.23a). The diameter of the ring corresponded to the SmA layer spacing. Below 62.7°C, the ring started expanding indicating that the molecules were now tilted with respect to the smectic layer normal. The ring appeared less intense as compared to that got from the TGB_A phase (Fig. 4.23b) for the same exposure time of $120min$. When the temperature was further lowered to below $59.0°C$, four intensity maxima appeared superimposed on the continuous ring (Fig. 4.23c). This could be due to a surface induced unwinding of the SmC^* helix near the glass plates (Fig. 4.23d). The above patterns were reproduced on heating also. Under the microscope it was noticed that in the intermediate phase there were several domains having different orientations of the square-grid pattern within the exposed region. Also, the resolution that could be achieved was very limited owing to the large beam cross-section. Due to these reasons it was impossible to verify whether the TGB structure in the new phase was commensurate or otherwise. The experiment was later repeated using the rotating anode generator. Even a beam size as small as ~ 200 x $200\mu m$ produced continuous diffraction rings in the intermediate phase as well as the TGB_A phase.

4.2.8 Electric field experiments

The response of the new structure to an externally applied electric field in various geometries was studied in some detail. Before going into the experimental observations we first give a brief description of the various effects of an external electric field on tilted smectics made up of chiral molecules.

As was pointed out by Meyer et al. [5], the C_2 point-symmetry of a tilted-smectic phase made of chiral molecules allows the medium to sustain a permanent polarisation. This polarisation is along a direction perpendicular to the plane containing the c-vector and the layer normal, N. Because the c-vector precesses along the layer normal, the medium is helielectric. Under the influence of an external field,

this permanent polarisation couples to the field linearly. Apart from this, there is also a coupling of the field to the director orientation which is quadratic in the applied field. This quadratic part is due to the anisotropy in the dielectric constants of the medium. Within each layer the medium can be assumed to be uniaxial with dielectric constants $\epsilon_{||}$ parallel to the director and $\epsilon_{\perp}$ perpendicular to the director. The dielectric anisotropy is usually defined as $\epsilon_a = \epsilon_{||} - \epsilon_{\perp}$. With the electric displacement vector written as

$$\mathbf{D} = \epsilon_{\perp}\mathbf{E} + \epsilon_a(\hat{\mathbf{n}} \cdot \mathbf{E})\hat{\mathbf{n}} \,, \tag{4.8}$$

the electric part of the free energy density is

$$\begin{aligned} f_{elec} &= -\mathbf{P} \cdot \mathbf{E} - \frac{1}{4\pi}\int \mathbf{D} \cdot d\mathbf{E} \\ &= -\mathbf{P} \cdot \mathbf{E} - \frac{\epsilon_{\perp}}{8\pi}\mathbf{E}^2 - \frac{\epsilon_a}{8\pi}(\hat{\mathbf{n}} \cdot \mathbf{E})^2 \,. \end{aligned} \tag{4.9}$$

The direction of $\mathbf{P}$ depends on the direction of c. The first term in Eq. (4.9), being linear in E, prefers an orientation of the director such that $\mathbf{P}$ is along E. If the direction of the field is reversed, the tilt direction will try to 'flip' ($\boldsymbol{c}$ will change sign) to minimise this term. The second term has no orienting effect on the director. The effect of the third term depends on the sign of ϵ_a. For $\epsilon_a > 0$, the director would prefer to align parallel to the field and for $\epsilon_a < 0$, it would like to lie in a plane perpendicular to the direction of the electric field.

The dielectric response can have contributions from two independent modes, namely, the *soft mode* and the *Goldstone mode*. The former arises due to the fluctuations in the magnitude of the tilt angle, whereas, the latter is due to the fluctuations in the direction of the tilt. The soft mode, as the name suggests, becomes prominent close to the $SmA - SmC^*$ transition due to the 'softening' of the relevant elastic modulus. Its contribution below the transition point is negligible compared to that from the Goldstone mode. The Goldstone mode has a relaxation frequency which is typically about $1kHz$. At frequencies much higher than this and well below the

$SmA - SmC^*$ transition point, the response of the director is completely dominated by the dielectric part. Also, at higher frequencies ($> 1kHz$) heating due to motion of ionic impurities is reduced. Due to these reasons a high frequency ($10kHz$) field was used in most of the studies.

In the case of cells treated for planar alignment an alternating electric field with a frequency of $10kHz$ was applied between glass plates coated with indium tin oxide (ITO). In this geometry, the field was acting along the TGB twist axis. Also, note that both the components of the mixture have negative dielectric anisotropies ($\epsilon_a < 0$). In the case of the square-grid texture, as the field was increased, the grid lines became narrow and straight. But faint and very fine lines remained even at fields as high as $\sim 30V/\mu m$ in a cell with $\sim 10\mu m$ thickness at 60.0^oC (see Figs. 4.24a,b). When the field was switched off the original texture was recovered almost immediately. No effects of any heating due to the electric field could be observed. It was also seen that the grid spacing first increased a little and then reduced continuously with increasing field. Plots of the lattice spacing as a function of the applied field for two different temperatures are shown in Fig. 4.25. This variation in the grid spacing cannot be due to any heating of the sample by the field as the spacing increases as the temperature is increased (see Sec. 4.2.6). The spacings were measured by the laser diffraction method. As was expected for this geometry, the electric field produced no observable effect on the TGB_A phase. This was because in the case of TGB_A even in the absence of any external field the Frank-director is almost everywhere parallel to the plane of the cell, the orientation favoured by an external electric field.

In the case of filaments in cells treated for homeotropic alignment, a similar alternating field was applied between the ITO coated plates. In this case, both the TGB_A as well as the corrugated filaments responded to the field because the field was applied perpendicular to the TGB twist axis. The filament width increased

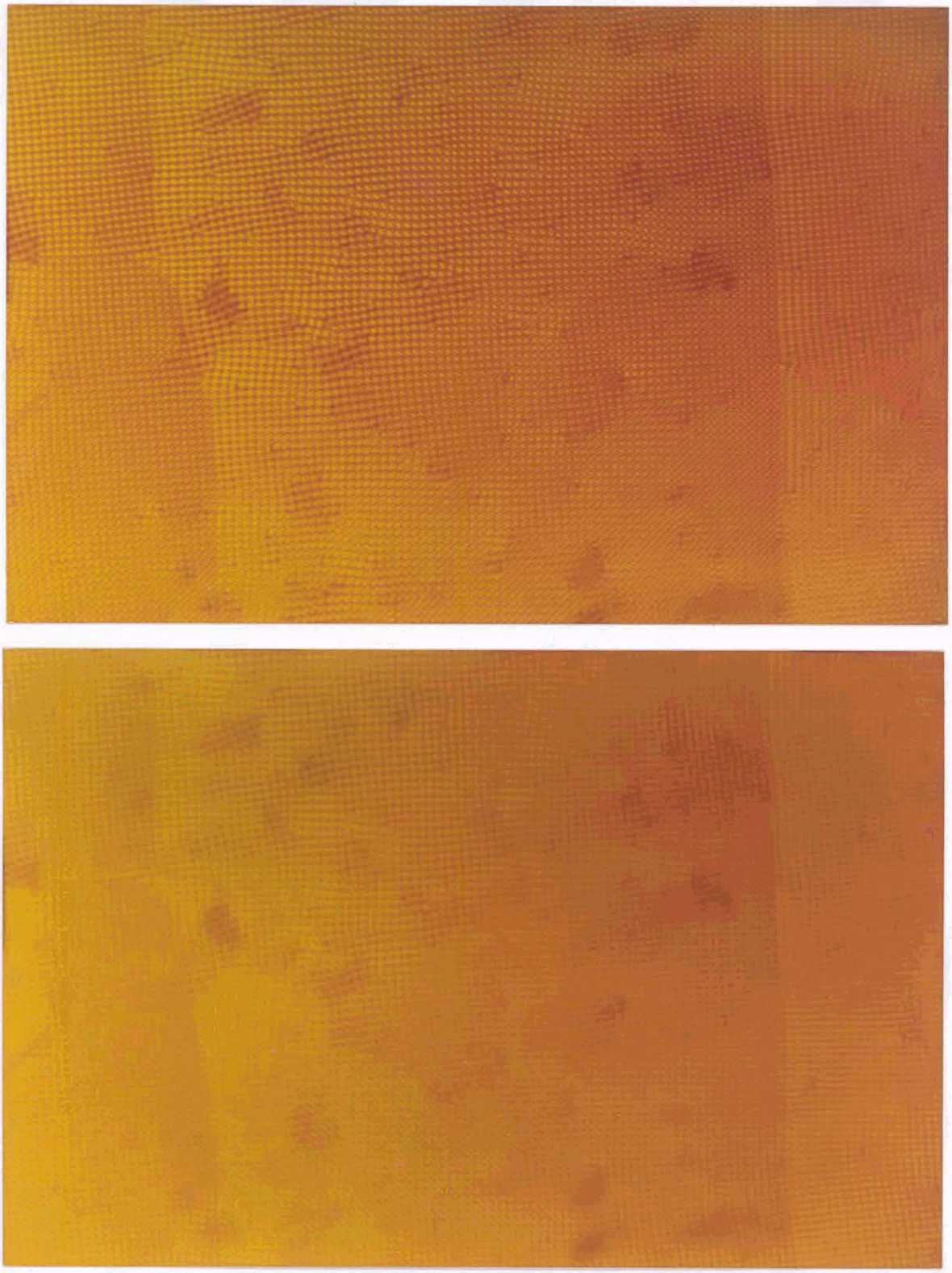

Figure 4.24: Photographs of the square grid texture in a $10\mu m$ planar aligned cell (a) without any external electric field and (b) with a $10kHz$ field of $\sim 15V/\mu m$.

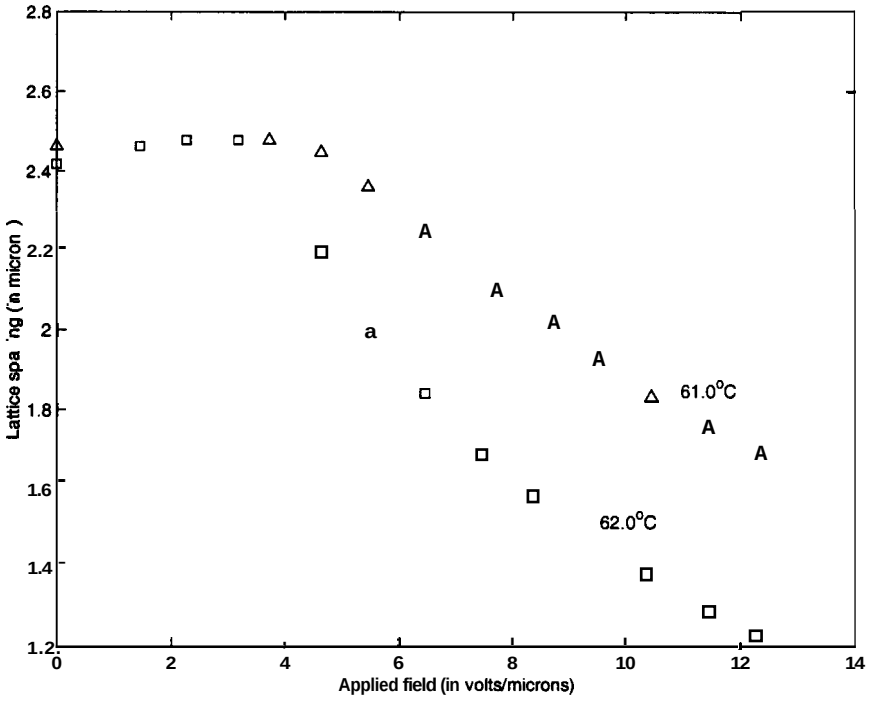

Figure 4.25: Variation of the lattice spacing of the square grid modulation as a function of applied field at two different temperatures. The cell spacing was $10.7\mu m$.

considerably when the field was raised to about $5V/\mu m$. The TGB_A filaments had a continuous dark line running along their middle. This was best seen when the polariser was set parallel to the filaments. In the new phase, under a similar field, the corrugated filaments became broader and more or less straight. The broadened filaments showed sharp intensity modulations along their lengths (see Figs. 4.26). On reducing the frequency to 1Hz, this intensity modulation responded at the frequency of the applied field. The widened filaments did not regain their original shape when the field was switched off (within about $20min$).

The electric field experiments can be understood if we assume the TGB blocks of the new phase to be SmC^*-like. In order to understand this let us first consider a uniform SmC^* structure under the influence of an alternating electric field applied parallel to the smectic layers. We assume that the frequency of the applied field is well above the relaxation frequency for the polarisation response. Therefore, only the dielectric part has an orienting influence on the director. Since the medium has

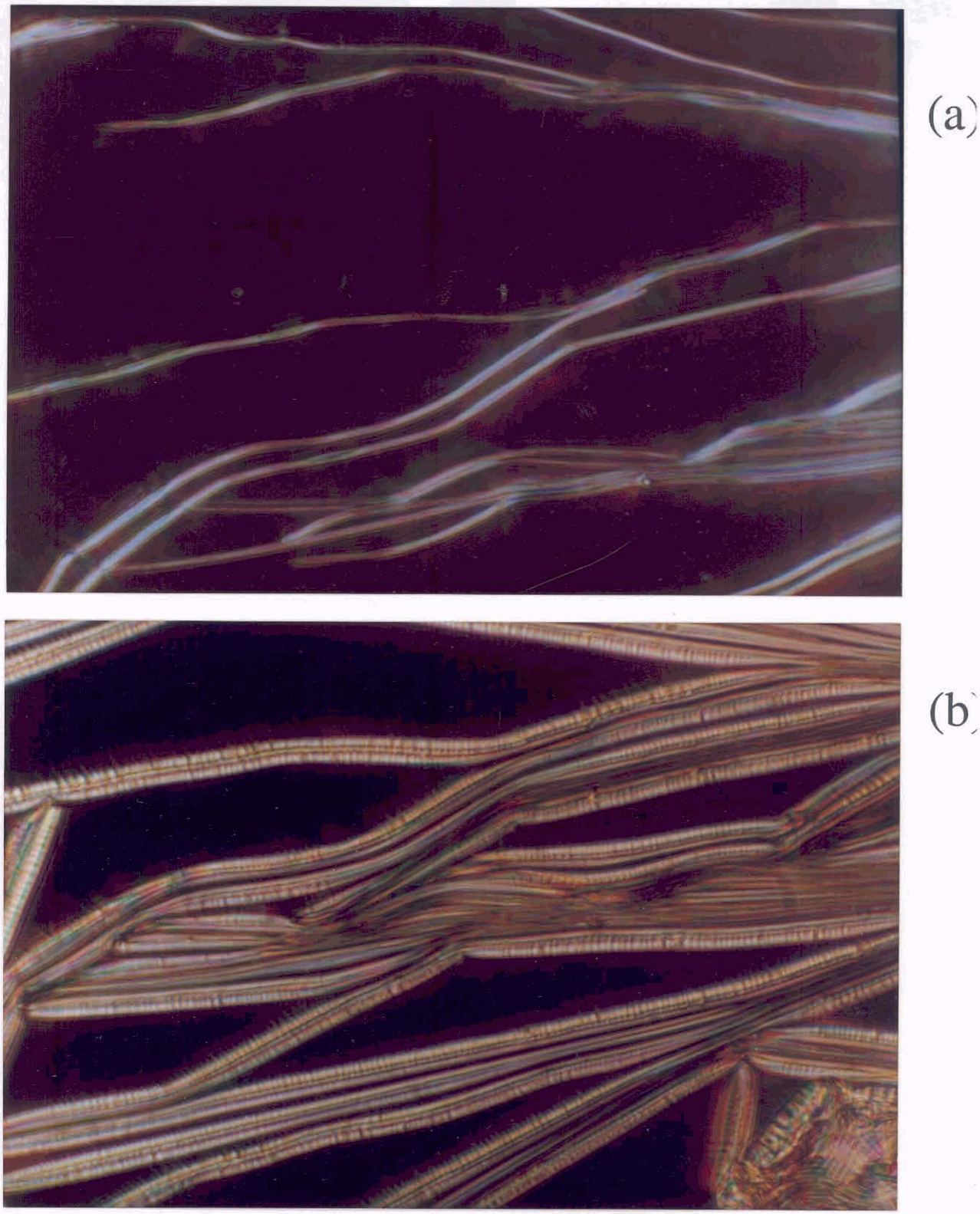

Figure 4.26: (a) The TGB_A filaments in the absence of any external field and (b) after the same region was cooled to the new phase and a field of $\sim 5V/\mu m$ was applied between the ITO coated plates.

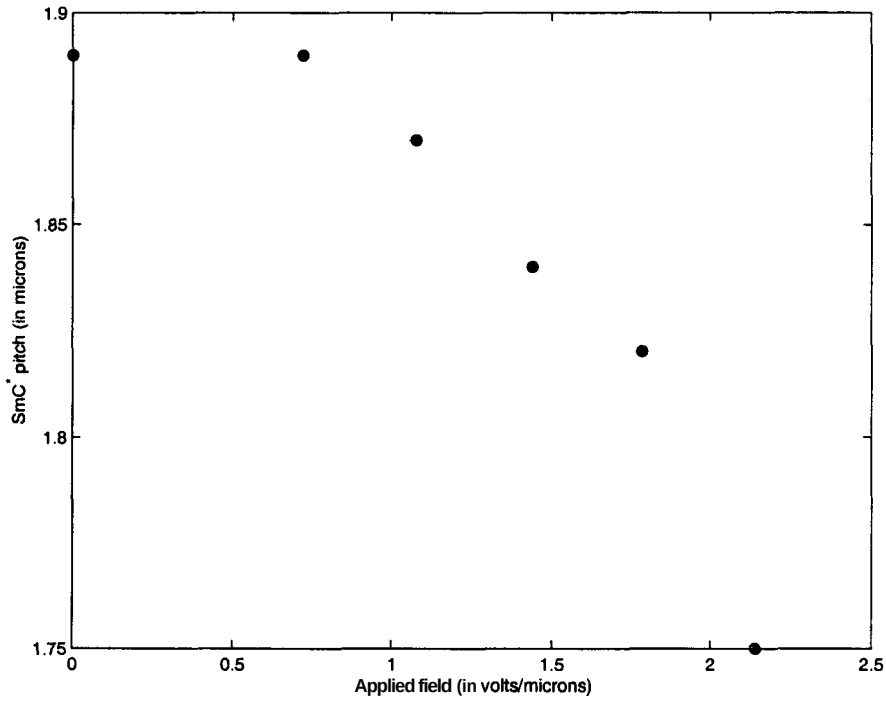

Figure 4.27: Variation of the SmC^* pitch of pure $CE8$ as a function of applied field. The sample temperature was 80.0^oC and the cell spacing was $11.0\mu m$.

---

a negative dielectric anisotropy ($\epsilon_a < 0$) in the SmC^* phase [48], the field favours regions where the director is in a plane perpendicular to it. For the SmC^* structure such regions occur with a periodicity which is equal to ***half*** the SmC^* pitch Fig. 4.28a. As the field strength is increased, these regions expand to reduce the electric part of the total free energy and the SmC^* twist is confined to narrower and narrower regions Fig. 4.28b. This produces a lattice of 'twist walls' (soliton lattice). Across each wall the c-vector rotates by π radians. Under the microscope the undistorted $(\mathrm{E} = 0)$ SmC^* structure shows periodic striations (pitch-lines). When the field is applied, these striations become narrower depending on the strength of the field due to the formation of twist walls. Experimentally, it is seen that these narrow lines remain even at fields as high as $100V/\mu m$ [59]. Unlike in cholesterics, the field does not unwind the twist in the structure completely.

We speculate that the narrowing of the grid lines is due to a similar effect occurring within the TGB blocks which have a SmC^*-like structure. This argument

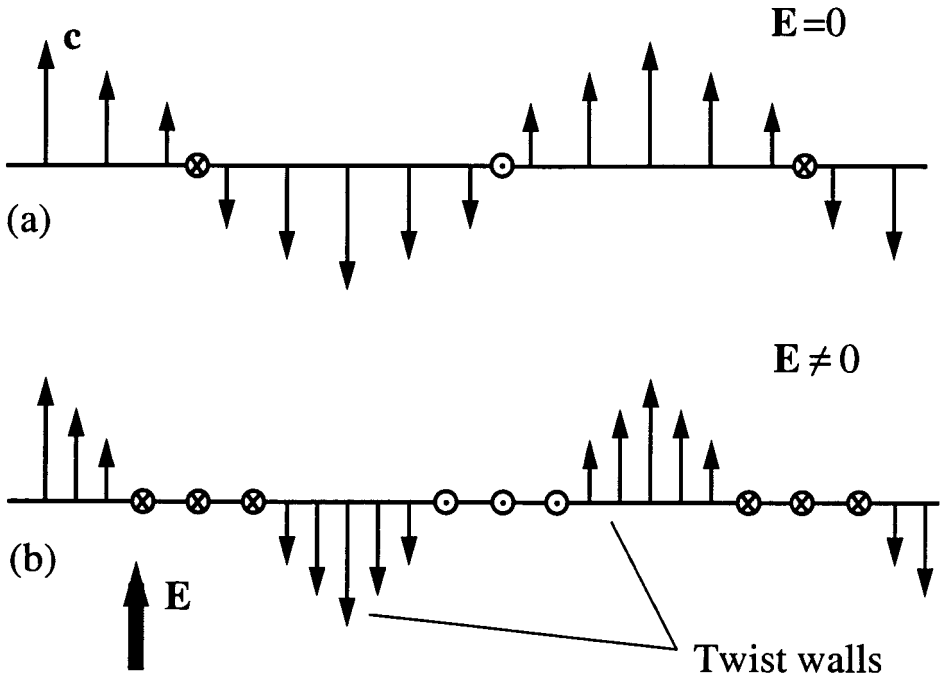

Figure 4.28: A schematic representation of the c-vector field in (a) an undistorted SmC^* structure and (b) a SmC^* structure under the influence of a high frequency electric field applied perpendicular to the twist axis and in the plane of the paper.

---

is further supported by the observation that the lattice spacing variation of the square grid Fig. 4.25 and the variation of the SmC^* pitch of pure CE8 Fig. 4.27, as a function of the applied voltage, shows very similar trends. The two spacings were measured by the laser diffraction method described in an earlier section. In the case of the square grid, the cell thickness was $11.0\mu m$ and for pure CE8 it was $10.7\mu m$. The frequency of the applied voltage was $10kHz$. In the case of the SmC^* pitch, measurements could be made only up to about 23V beyond which electrohydrodynamic motion [1] produced undesirable effects.

4.2.9 Electrooptic experiments

As mentioned in the previous section, the chiral medium can sustain a permanent polarisation when the molecules are tilted with respect to the smectic layer normal. This makes it very easy to excite the molecules by applying an external electric

field. The response of the molecules will depend on the structure of the medium apart from the tilt angle, viscosity, elastic constants, etc. Furthermore, the high birefringence of these systems makes it easy to detect small changes in the structure by optical methods. Thus, electrooptic measurements are very useful in detecting structural changes and studying mechanical properties of such systems.

The electrooptic measurements were conducted on $\sim 4pm$ thick, aligned samples in the planar geometry. The sample temperature was controlled by an Instec hot-stage and controller which has an accuracy of $\pm 5mK$. The sample temperature was measured using a Minco platinum resistance thermometer mounted very close to the sample. The hot-stage was mounted on a microscope stage to allow visual verification of the sample alignment. The light from an ***He-Ne*** $(632.8nm)$ laser beam was first divided into two beams using a beam-splitter and one of them was allowed to pass through the sample kept between crossed polarisers. The transmitted intensity was measured using a PIN photodiode mounted on the microscope. The second beam was used as a reference to monitor and correct for fluctuations in the input laser intensity. An alternating voltage of $4.9V$ at $403Hz$ derived from the internal oscillator of a lock-in-amplifier was applied across the ITO coated glass plates of the cell. The cell was oriented with the rubbing direction at 45^o with respect to the polariser and the analyser. The current through the photodiodes was converted into voltage signals and measured using the lock-in-amplifier. The entire experiment was controlled using a personal computer. A schematic diagram of the experimental set-up is shown in Fig. ***4.29.***

The variation in the first harmonic of the electrooptic signal measured as a function of the sample temperature is shown in Fig. ***4.30.*** Since the TGB_A phase has no net polarisation, the signal from this phase is almost zero. The signal starts increasing very close to the transition to the new phase. There is a maximum in the signal within the temperature range of the new phase. This can be seen in both

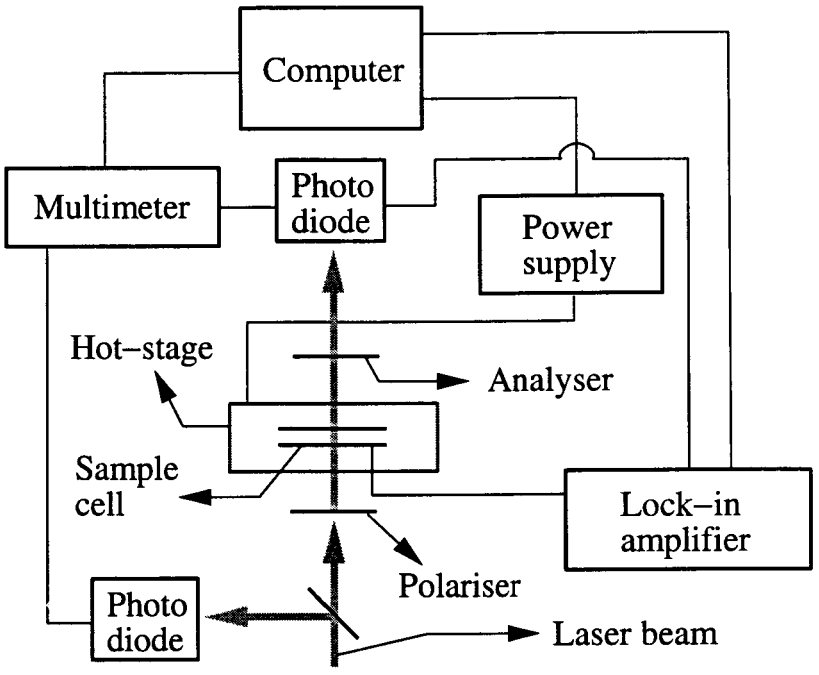

Figure **4.29: A** block diagram of the set-up used for the electrooptic experiments.

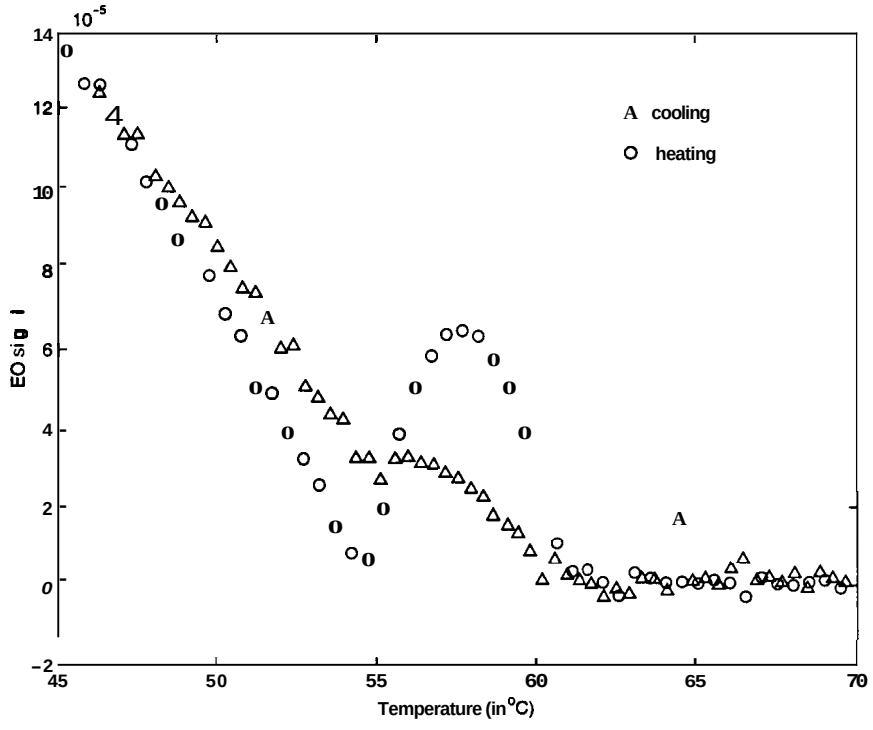

Figure **4.30:** The electrooptic signal measured as a function of temperature during cooling and heating runs. The cell was oriented such that the rubbing direction was at 45^o with respect to the crossed polarisers. The cell thickness was $4.6\mu m$, and the applied voltage was $4.9V$ at a frequency of $403Hz$.

heating and cooling runs though the exact shape of the curves are different. The transition to the SmC^* phase is marked by a minimum in the signal level. In the SmC^* phase the signal steadily increases with decrease in the temperature.

4.3 Proposed structure for the new TGB phase

From the experimental results described in the previous sections, we come to the following conclusions about the new phase.

- The presence of the Grandjean-Cano lines in the wedge shaped cells, the filamentary growth in the homeotropic cells and the smectic like peaks got from xray diffraction indicate that the new phase is a twist grain boundary phase.

- The layer spacing measurements and the electrooptic measurements show that the molecules are, on the average, tilted with respect to the smectic layer normal.

- The corrugated nature of the filaments as well as the pitch-lines and the square lattice modulation in the planar case together indicate that the grain boundaries separating the smectic blocks have a two-dimensionally undulating structure.

- The experiments on the corrugated filaments show that the projection of the Frank-director on to the plane of the cell is parallel to the local filament orientation (near the central region). A SmC^*-like structure for the blocks is compatible with this arrangement and does not require any layer distortions (Fig. 4.31a). If one assumes that the blocks are SmC-like, the above condition cannot be met without layer compressions and dilations (Fig. 4.31b) which are energetically very expensive [1, 2].

- The response of the structure to an external electric field can be understood if

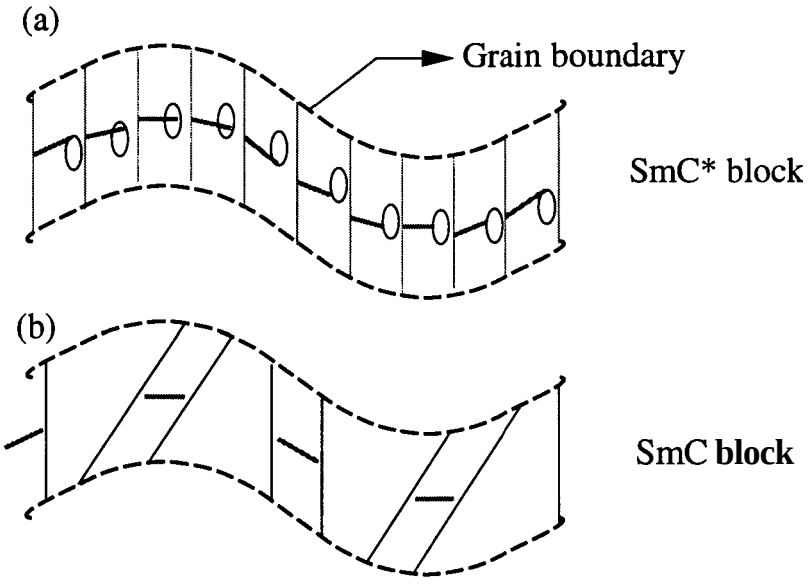

Figure **4.31:** A schematic drawing of blocks with (a) SmC^*-like and (b) SmC-like structure. Both structures satisfy the condition that the projection of the frank director is parallel to the local filament orientation. But in the case of SmC-like blocks, this can be achieved only by introducing layer compressions and dilations.

---

one assumes that the TGB-blocks have a SmC^*-like structure. This supports the previous argument

Thus, this *three-dimensionally modulated* structure has twist distortions along three mutually orthogonal directions. This is reminiscent of the blue phases exhibited by short-pitch cholesterics close to the transition to the isotropic phase (see Sec. 1.3.1). The periodicity along the TGB twist axis is in general different from the lattice spacing of the modulation in the orthogonal plane. This structure with the undulating grain boundaries was not anticipated by any of the theoretical models. Since the grain boundaries of this new phase has a two-dimensionally undulating character, we call this the Undulating TGB_{C^*} phase or the $UTGB_{C^*}$ phase for short.

A schematic diagram of the structure proposed for the $UTGB_{C^*}$ is shown in Fig. **4.32.** The shaded surfaces represent the two-dimensionally undulating grain boundaries. Note that all the grain boundaries undulate along the same two directions. This is required if the block thickness has to be maintained uniform. The

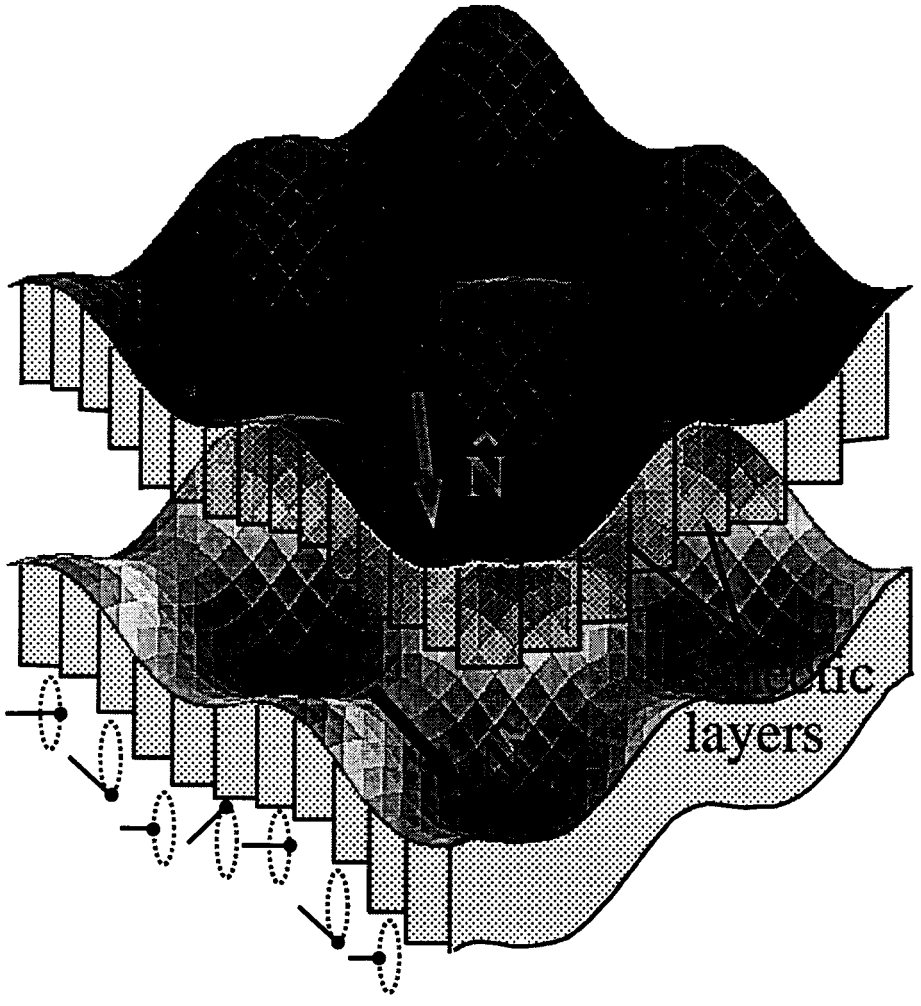

Figure **4.32:** A schematic representation of the proposed structure for the $UTGB_{C^*}$ phase. The shaded area represents the two-dimensionally undulated grain boundary region. The smectic layer normals (large arrows) rotates from block to block. Within each block the Frank-director precesses along the layer normal direction as represented by the nails.

fact that the net optical pattern shows modulations only along two orthogonal directions supports this argument. The smectic layer normal, however, rotates on passing from one block to another as in the TGB_A phase. Within each block, the c-vector precesses about the layer normal to form a SmC^*-like arrangement.

A possible physical origin of the undulating grain boundaries and a model for explaining the occurrence of the $UTGB_{C^*}$ phase are discussed in the next chapter.

4.4 Conclusion

We have presented the details of the experimental observations of a new liquid crystalline phase. This phase, which belongs to the Twist Grain Boundary (TGB) class of liquid crystalline phases has a structure which is far more complicated than that of the TGB_A and the TGB_C phases. The experiments described in this chapter show that this structure is three-dimensionally modulated with twist-axes along three mutually orthogonal directions.

More recently there have been reports of experimental observations of similar textures in some pure compounds [60, 61] as well as mixtures [47]. More detailed experiments are needed to understand this highly non-uniform structure in greater detail. In the next chapter we present a simple theoretical analysis to explain the occurrence of this highly complex state.